UNIVERSIDAD MICHOACANA DE SAN NICOLAS DE HIDALGO

DIVISIÓN DE ESTUDIOS DE POSGRADO
FACULTAD DE INGENIERÍA QUÍMICA

Geological Earth and Waste Industrial Materials In Production of Eco- Friendly Cement Low CO_2 Emissions and Low Global Warming

TESIS presentada por:

HASSAN SOLTAN HASSAN MOHAMED IBRAHIM

A la División de Estudios de Posgrado de la Facultad de Ingeniería Química como Requisito parcial para obtener el Grado de:

DOCTOR EN CIENCIAS

EN

INGENIERÍA QUÍMICA

ASESOR: Dr. Salomon Ramiro Vasquez Garcia

MORELIA, MICHOACAN, MEXICO. **Febrero 2021**

Geological Earth and Waste Industrial Materials In Production of Eco-Friendly Cement Low CO_2 Emissions and Low Global Warming

ABSTRACT

Since the beginning of the creation of man in the universe and when he started his activities, the earth began to suffer. These activities created pollutant environments due to high emission of the carbon dioxide and increase the global warming. From the major activities responsible for produce of high quantities CO_2 emission on earth is the Cement manufacturing. This single industry accounts for more than 5% of global man-made CO_2 emissions; the amount of CO_2 emitted by the cement manufacturing is nearly 950 kg of CO_2 for every 1000 kg of cement produced. The team of investigation is aiming to eliminate these polluted emissions and decrease global warming by using different novel techniques utilizes both natural earth (Geologic materials) and waste industrial materials. A new different type of friendly environmental cementitious binder (Geopolymer Cement) with outstanding properties in hardness, fire and Corrosion resistant has been done, On the other hand, the utilization of waste industrial materials creates clean green environments.

Keywords: Global warming, Geopolymer Cement, Cement Industry, CO_2 emissions, Geologic materials.

DEDICATIONS

I would like to dedicate this simple work to my Dad Mr. Soltan Hassan Mohamed and my mom Mrs. Fatma El-Salamony whom bring me to this life and raise me up until I become an independent and responsible man. Also, brother Captain Military Engineer Mohamed Soltan Hassan and my sister's Randa Soltan Hassan and Nessma Soltan Hassan.

A special dedication to my beautiful and faithful lady my wife, Dra. Fatma El-Zahraa Moustafa. She stands by my side in every step of my life. My beautiful two angels Mazen and Omer Hassan Soltan Hassan also a special dedication to them. I wish one day to see and attend your doctorate degree.

Finally, I would like to dedicate this simple work to my brother, Professor and friend Dr. Salomon Ramiro Vasquez Garcia. He stands by my side in every step during achieving this simple work.

ACKNOWLEDGMENTS

I would like to thank my beautiful family my Dad Mr. Soltan Hassan Mohamed and my mom Mrs. Fatma El-Salamony whom brought me to this life and raise me up until I become an independent and responsible man. I deeply appreciated their efforts to raise me up. Thanks, my beautiful Mom and Dad I am owing you both a lot, May God bless and protect you forever.

Thanks so much for my beautiful lady, Dra. Fatma El-Zahraa Moustafa. My beautiful wife for her faithful efforts during all my life. Another beautiful acknowledgment to my beautiful angels Mazen and Omer Hassan Soltan Hassan for their support during my challenge in Mexico.

Another acknowledgment to my best friend, Brother and my Professor Dr. Salomon Ramiro Vasquez Garcia. For his support and standing by my side during this big challenge in Mexico. Indeed, it was an honor and pleasure to work under your supervision.

A special gratitude to my beautiful Dra. Nelly Flores-Ramirez for her support during this mission in Mexico, Also to Drs. Jose L Rico and Marco Antonio Martinez-Cinco for their faithful efforts with me.

Thanks so much to Dra. Isabel Israde-Alcántara, for her support in every project we did. Indeed, it was an honor to work with her during all the project we accomplished together

NOMENCLATURE

GPC Geopolymer Cement; GW Global warming: CM Cement Industry: VA Volcanic ashes; CO2-capture; MBC Magnesia-based cement; CA Coconut ash; TC Thermal conductivity; CS Compressive strength; AS Alumina slag; FA Foaming agent; WBA Wood biomass ash; Diatomite; OPWGC One-part white geopolymer cement.

TABLE OF CONTENTS

LIST OF FIGURES

LIST OF TABLES

LIST OF Diagrams

CHAPTER I
INTRODUCTION

1.1. General Background

The term of geopolymer was invented by **Davidovits (1988)**. Geopolymeric materials can be synthesized by mixing alkaline solution with aluminosilicate materials. The most common aluminosilicate materials used in the fabrication of geopolymer are naturally-occurring materials and industrial solid wastes. Fly ash (FA), and ground granulated blast-furnace slag (GGBFS) are the main industrial byproducts used in geopolymer synthesizes **(Ma et al., 2018; Wang et al., 2017; Jayaranjan et al., 2014; Saravanan et al., 2013; Duxson and Provis, 2008; Abdel-Gawwad et al., 2016; Abdel-Gawwad and Abd El-Aleem, 2015)**. The naturally occurring mainly includes kaolinitic clay (namely kaolinitic clay) which was previously used as aluminosilicate precursor in geopolymer synthesizes **(Davidovits, 2013)**. Before utilizing kaolinitic clay in geoplymer making, it should be thermally-treated at temperature range of 500-800ºC. The thermal treatment was found to have a potential impact on the transformation of crystalline kaolinitic clay into amorphous metakaolin (MK). Other researchers have used the hybrid naturally-occurring materials and industrial byproduct in geopolymer production including MK/GGBFS **(Abdel-Gawwad et al., 2016)** and MK/FA (**Kuenzel et al., 2014**).

Alkali activators which were used to induce the geopolymerization reaction are sodium hydroxide (**Matalkah et al., 2017**), potassium hydroxide **(van Deventer et al., 2010)**, sodium silicate (**Luukkonen et al., 2018)**, sodium aluminate (**Sturm et al., 2016**) sodium carbonate **(Kovtun et al., 2015)**, and sodium sulfate **(Garcia-Lodeiro et al., 2016)**.

Geopolymerization process includes three main steps, i.e. dissolution, condensation and polymerization **(Davidovits, 2015; Komnitsas and Zaharaki, 2007)**. The dissolution of aluminosilicate precursors induced after their mixing with alkaline solutions, resulting in the formation of aluminate, silicate, and aluminosilicate activated species or monomers **(Duxson et al., 2007)**. Condensation process of these monomers occurred at the same time of dissolution stage, yielding two-dimensional aluminosilicate chains in the sequence of Si-

O-Si-O-Al or Si-O-Al-O-Si depending on the alumina to silica molar ratio (**Davidovits, 1988**). Finally, the polycondensation of these aluminosilicate chains (at 25-90ºC) has resulted in the formation of three-dimension aluminosilicate polymer with high mechanical properties.

The main parameters which strongly affect the performance of geopolymer are alkaline concentrations and types and **(Ma et al., 2018; Luukkonen et al., 2018; Rashad et al., 2016; Abdel-Gawwad et al. 2016; Torres-Carrasco and Puertas, 2017; Hadi et al., 2018)**, curing conditions **(Haque et al., 2018; Hwang et al., 2018),** chemical composition, and physical properties of the starting materials **(Němeček et al., 2011)**. Generally, geopolymeric materials demonstrated higher mechanical properties (**Thomas et al., 2018; Abdel-Gawwad et al., 2018a,b; Abdel-Gawwad and Khalil 2018; Abdel-Gawwad et al., 2016; Abdel-Gawwad and Abd El-Aleem, 2015)** as well as higher resistivity towards aggressive media, acid **(Bakharev et al., 2003; Bakharev, 2005; Temuujin et al. 2011; Sturm et al., 2018)**, firing **(Zhang et al., 2014; Rashad and Khalil, 2013; Zuda et al., 2006)**, and freeze-thaw **(Topçu et al., 2014; Fu et al., 2011)** compared to Portland cement. Furthermore, geopolymers strongly contribute to mitigate the environmental pollution (CO_2-emmision) resulted from Portland cement production **(McLellan et al., 2011; Habert et al., 2011; Bagheri et al., 2018).**

Geopolymers have been widely used in different applications such as thermally-insulating materials (**Zaidi et al., 2017)**, firing resistance inorganic materials (**Saxena et al., 2017**), decorative and foundry works **(Davidovits 2015)**, refractories **(Bakri et al., 2013)**, biological applications **(Catauro et al., 2010)**, concrete repairing **(Ding et al., 2017)**, cements and concretes **(Sikandar et al., 2019)** radioactive and toxic waste containment (**Abdel-Gawwad et al., 2019b; Xu et al., 2017**).

Although advantageous of geopolymers, they represented the main disadvantage including their lower commercial viability compared to Portland cement. This mainly shortcoming originated from the high corrosive nature of alkaline solutions. Several authors proposed new approaches to produce user-friendly one-part geopolymer which can react with water like Portland cement.

1.2. Aim and Goal

This study aims to decrease the CO_2 emissions from the cement industry by utilizing of both natural and waste industrial alumino-silicates materials in production of Geopolymer Cement (GPC) with highly mechanical properties. Also, in order to enhance the mass production of Eco-friendly Geopolymer cement (Environmentally Green Friendly Cement). Another important aim in this investigation is to create some outstanding features to this GPC, for instance make it extremely durable, resistance for fire and acids corrosions and the ability to adsorb the CO2 from the air in both long and short terms.

The goal of the work is to create an eco-friendly cement material (Geopolymer Cement) at room temperature with outstanding mechanical and non-mechanical properties for instance (High compressive strength, high durability, high resistance for fire and acid corrosions, high thermal insulation property and finally the ability to adsorb CO2 from the air in both short and long terms

1.3. Objectives

General Objective

To decrease the CO_2 emissions from Cement manufacturing by creating new cementitious materials with outstanding mechanical properties.

Specific objectives

1.3.1- Cleaner production of one-part white geopolymer cement using pre-treated wood biomass ash and diatomite.

1.3.2- The potential application of eco-friendly magnesia-silicate cement in CO2 sequestration.

1.3.3- The creation of a geopolymer foam with high thermal insulation properties from Coconut ashes wastes.

1.4. Hypothesis

The utilization of suitable activators like (NaOH or NaSiO2) to activate the aluminum silicates materials a combined with a specific types of some substance as MgO, Aluminum powder, and Coconut waste lead to a new cementitious materials with variable for instance mechanical and non-mechanical properties (High compressive strength ranging from 80-90MPa in 28 days, acid and fire resistance, high thermal insulation and with ability to absorb the CO2 from the air in both (long and short terms).

1.5. Justifications

From the major activities responsible for produce of high quantities CO_2 emission on earth is the Cement manufacturing. This single industry accounts for more than 5% of global man-made CO_2 emissions; the amount of CO_2 emitted by the cement manufacturing is nearly 950 kg of CO2 for every 1000 kg of cement produced. The team of investigation is aiming to eliminate these polluted emissions and decrease global warming by using different novel techniques utilizes both natural earth Geologic materials and waste industrial materials, to produce an eco-friendly cement as Geopolymer cement equal or more in properties like the OPC (Ordinary Portland cement).

CHAPTER II
LITERATURE REVIEW

2.1. Geopolymers and History

Geopolymers are inorganic aluminosilicate polymers that form solid ceramic-like materials at near ambient temperatures. Geopolymeric materials can be synthesized by mixing alkaline solution with aluminosilicate materials. The most common aluminosilicate materials used in the fabrication of geopolymer are naturally-occurring materials and industrial solid wastes. Fly ash (FA), and ground granulated blast-furnace slag (GGBFS) are the main industrial byproducts used in geopolymer synthesizes **(Ma et al., 2018; Wang et al., 2017; Jayaranjan et al., 2014; Saravanan et al., 2013; Duxson and Provis, 2008; Abdel-Gawwad et al., 2016; Abdel-Gawwad and Abd El-Aleem, 2015)**.

2.2. Geopolymer Synthesis

In general Geopolymer has been synthesized by the activation of different aluminum silicates material using different strong activators NaOH, Na_2SiO_3, MgO, CaO and many other activators. Geopolymerization process includes three main steps, i.e. dissolution, condensation and polymerization **(Davidovits, 2015; Komnitsas and Zaharaki, 2007)**. The dissolution of aluminosilicate precursors induced after their mixing with alkaline solutions, resulting in the formation of aluminate, silicate, and aluminosilicate activated species or monomers **(Duxson et al., 2007)**. Condensation process of these monomers occurred at the same time of dissolution stage, yielding two-dimensional aluminosilicate chains in the sequence of Si-O-Si-O-Al or Si-O-Al-O-Si depending on the alumina to silica molar ratio (**Davidovits, 1988**). Finally, the polycondensation of these aluminosilicate chains (at 25-90ºC) has resulted in the formation of three-dimension aluminosilicate polymer with high mechanical properties.

2.3. Microstructure of Geopolymers

Geopolymerization is the process of combining many small molecules known as oligomers into a covalently bonded network. The geo-chemical syntheses are carried out through oligomers (dimer, trimer, tetramer, pentamer) which provide the actual unit structures of the three-dimensional macromolecular edifice. **In 2000, T.W. Swaddle** and his team proved the existence of soluble isolated alumino-silicate molecules in solution in relatively high concentrations and high pH. One major improvement in their research was that their study was carried out at very low temperatures, as low as −9 °C. Indeed, it was discovered that the polymerization at room temperature of oligo-sialates was taking place on a time scale of around 100 milliseconds, i.e. 100 to 1000 times faster than the polymerization of ortho-silicate, oligo-siloxo units. At room temperature or higher, the reaction is so fast that it cannot be detected with conventional analytical equipment.

In general the structure of the normal geopolymer consists of, soluble oligomers of the K-poly(sialate) / poly(sialate-siloxo) species, which are the actual starting units of potassium-based alumino-silicate geopolymerization.

2.4. Mechanical Properties of Geopolymers

Geopolymers, characterized by its high mechanical properties (extremely high compressive strength), corrosion resistance, low thermal conductivity, low sound conductivity, very isolated material, durability, especially desirable performance under high temperature, wide source of raw materials, and low energy consumption. Geopolymers has become an increasingly popular research area in recent years. It is considered to be potential substitutes for Portland cement. Consequently, geopolymers have wide applications in fields such as toxic chemical wastes absorption, ultraviolet radiation resistance, and drug delivery. They are also widely used in lightweight concrete and foam concrete for the superior insulation properties. For example, **Arellano Aguilar et al.** prepared lightweight concrete with 50% lower density compared with the conventional cement concrete by using MK and FA geopolymers. **Zhang et al.** prepared heat reflective and thermal insulation coating by using the MK geopolymers and found that the heat reflectivity of the prepared coating exceeded 90% and the thermal insulation temperature difference was 24°C.

2.5. State of the Art

The main feature of one-part geopolymers is the high hydration reactivity as they can react with water, yielding hardening materials with considerable compressive strength. This means that the preparation of one-part mixtures strongly enhances the mass production of geopolymer and resolving the corrosive nature of alkaline solution. several approaches have been implemented to create one-part geopolymer comprising the effect of different parameters on their properties.

2.6. Types of raw materials used in synthesizing one-part geopolymer

The most common aluminosilicate materials which were used in the preparation of one-part geopolymer are class-F fly ash (FA) from core combustion. It can be blended with slag to produce one-part geopolymeric material that can be hardened at room temperature **(Yang et al., 2008; Yang et al., 2009; van Deventer et al., 2010; Nematollahi et al., 2015; Wang et al., 2017; Nematollahi et al., 2017; Nematollahi et al., 2017; Hajimohammadi and van Deventer 2017)**. class-c fly ash (with high Ca content) has low efficacy in the production of one-part geopolymeric material due to rapid setting and less availability (**Chindaprasirtand et al., 2012; Rattanasak et al., 2011)**.

Ye et al., 2016 have prepared one-part geopolymer from FA and red mud (activated by NaOH) with high property in the solidification/stabilization of heavy metals; Meanwhile **Matalkah et al., 2017** have applied the mechanical and chemical activation in the production one-part FA- based geopolymer on. This was implemented by grinding CaO, MgO and NaOH with FA. They reported that Na, Ca and Mg ions where included in FA structure, resulting in an improvement in the properties of the prepared geopolymer Ca-rich aluminosilicate material (GGBFS) was used as one of the main precursors in the preparation of one-part geopolymer material. It can be mixed with FA or can be used alone (**Hajimohammadi and van Deventer 2017; Choo et al., 2016; Nematollhi et al., 2014; Hajimohammadi et al., 2010; Nematollhi and Sanjayan, 2016; Suwan and Fan, 2017; Nematollahi et al., 2017)**. GGBFS represented the potential effect on the reactivity of low Ca-FA (**Duxson and Provis, 2008**), as it induced rapid setting accompanied by high strength at early age (**van Deventer et al., 2010; Nematollahi et al., 2015; Wang et al.,**

2017; Nematollahi et al., 2017; Nematollahi et al., 2017; Hajimohammadi and van Deventer, 2017; Chindaprasirtand et al.,2012; Rattanasak et al., 2011; Ye et al.,2016; Matalkah et al., 2017; Temuujin et al., 2009; Djobo et al.,2016; Li et al., 2013). The partial replacement of slag with Ca $(OH)_2$ has resulted in a remarkable decrease in compressive strength and workability of one-part geopolymer (**Nematollahi et al., 2015)**. The fineness of slag played on important role in the performance of one-part geopolymer. the decrease of particle size of slag. Positively reflects the compressive strength development of one-part geopolymer (**Yang et al., 2009)**. Slag and solid sodium silicate at 5:1 by weight was the optimum ratio to produce one-part geopolymer with the highest mechanical properties; Meanwhile the lower ratio (4:1) and higher ratio (6:1) have a negative effect on the performance of the prepared geopolymer (**Nematollahi et al., 2017**).complementary, The application of different slags caused the significant decrease in the value of slump, higher elastic modulus companied by higher tensile strength and less brittle structure (**Nematollahi et al., 2017)**. Fayalite slag as a byproduct of Cu or Ni is melting process (**Shi, 2017)** can be used in the preparation of one-part geopolymer by an innovative process in which fayalite slag dry mixed with maize cop ash followed by mixing with water (**Peys et al., 2017**). The naturally-occurring clay minerals also can be used as a good aluminosilicate ingredient in the production of one-part geopolymer. **van Deventer et al.,** (**2010)** have listed natural clays and other minerals that could be used in the preparation of one-part geopolymer. These minerals included potash, feldspar, albite, natural zeolite, fayalite and purophylite. Thermo chemically treated albeit as one-part geopolymer can be prepared by heating of albeit at 1000ºC in the presence of NaOH or Na_2CO_3, yielding highly reactive aluminosilicate material which can react with water to produce hardened material with high performance. As a byproduct of alumina manufacturing, red mud with high alumina, silica, iron and alkali content (**Paramuru et al.,2005)** has been used in the production of alkali activated binders (**Jamieson et al.,2016; Nie et al., 2016; Zhang et al., 2016)** and OPC (**Vangelatos et al.,2009; Tsakiridis et al., 2004**), Also red mud have been used in synthesizing one-part geopolymer after thermo chemical activation in the presence of NaOH (**Ye et al., 2016; Ke et al., 2015; Ye et al., 2016).** It can be used as alternative alkali activator for synthesizing one-part FA-based geopolymer (**Choo et al. 2016)**. **van Deventer et al., (2010)** also stated that all naturally occurring aluminosilicate

materials should be thermally treated before its using in the production of one-part geopolymers. Whereas, industrial aluminosilicate solid waste could be used with no pretreatment. **Abdel-Gawwad and Khalil (2018),** have prepared one-part geopolymeric material using the vitrification of cement kiln dust and feldspar at elevated temperature. They studied the impact of elevated temperatures and alkali concentrations on the performance of the produced geopolymeric material. They reported that the optimum one-part geopolymer can be produced at 1200ºC in the presence of NaOH concentration of 20 wt. %.

2.7. Alkali activator sources

The main action of alkali activator is the rising the pH of the media, leading to an enhancement the solution rate of aluminosilicate materials. Many activators such as NaOH, Na_2CO_3, $NaAl_2O_3$, Na_2SO_4, $CaSO_4$, Na_2SiO_3, KOH were used in the activation of hydration of one-part geopolymer (**Hajimohammadi et al., 2010; Suwan and Fan 2017; Koloušek et al., 2007; Peng et al., 2015; Abdel-Gawwad and Abo-El-Enein 2016; Nematollahi et al., 2015; Peys et al., 2017).,** Industrial solid wastes including red mud and maize stalk and cope ash have used as alternative alkali sources The SiO_2Na_2O ratio of Na_2SiO_3 has been used with variable values ranging from 0.93 to 3.32 in the previous published works which have studied one-part geopolymer preperation (**Wang et al., 2017; Nematollahi et al., 2017; Hajimohammadi and Van Deventer 2017)**. One-part FA-based geopolymer activated by Na_2SiO_3 in which SiO_2Na_2O molar ratio is 0.93 represented higher mechanical properties, and better workability than that of activated by Na_2SiO_3 with SiO_2Na_2O molar ratio 2.06 **(Nematollahi et al., 2015)**. **Choo et al., 2016)** have implemented an innovative method to create one-part geopolymer by mixing red mud (as NaOH source) with CaO, MgO, Ca $(OH)_2$ and dolomite (**Li et al., 2010).** Complimentary one-part geopolymer which prepared by mixing CaO with GGBFS demonstrates performance higher than that of Ca $(OH)_2$ activated slag. The main reason behind this effect is the high released heat resulted from CaO hydration (**Kim et al., 2013)**. All the above-mentioned activators represented disadvantages. Including the high corrosive and hygroscopic nature. Moreover, NaOH production is a toxic industry as it releases high Cl_2 content **(Provis et al., 2017; Glasby et al., 2015)**. On the other hand, the production of Na_2SiO_3 consumed high energy which

negatively effects on the environment (high CO_2 emission). Accordingly, the full replacement of synthesized Na_2SiO_3 with other alkali or silicate sources is mandatory. Trona is naturally-occurring mineral which with Na_2CO_3 can be used as efficient activator in synthesizing one-part geopolymer with performance comparable to that of activated by NaOH, especially at elevated temperature **(Obonyo et al., 2011; Peng et al.,2015; Peng et al., 2017**). Nevertheless, Na_2CO_3 was found to exhibit high CO_2 -emission at elevated temperature.

Accordingly, **Abdel-Gawwad et el., (2019), Hasson et al., (2019)** have prepared dry activator by the treatment of concrete waste and wood powder. The treatment process was conducted by mixing NaOH with Ca-rich-materials followed by drying and grinding to yield dry activator powder which mainly composed of Ca and Mg $(OH)_2$ as well as Na_2CO_3. One-part geopolymeric material were synthesized by mixing alumino-silicate materials with the prepared dry activator.

2.8. Addition of amorphous sources

Different sources of silica and alumina were admixed with precursors (FA, metakaolin, and slag) during the preparation of one-part geopolymer. Rice husk ash and rice hull are the residues of the agricultural waste combustion as they contain excessive amorphous silica content exceeding 90 wt. % **(Chandrasekhar et al., 2003; Della et al., 2002)**. These ashes were activated by solid sodium aluminate to create one-part geopolymer mixes **(Hajimohammadi and van Deventer 2016; Sturm et al.,2016)**. After addition of water and curing for 1-day the hardened material demonstrated compressive strength value of 30 MPa (**Sturm et al., 2016)**. associated with the full activated silicate constituent in ashes. In some cases, the ashes may contain unburned carbon **(Venkatanarayanan and Rangaraju 2013)**. Maize stalk and cop ashes are categorized as alkali silicate materials as they have 30 wt. % of K_2O and 20 wt. % SiO_2 and another constituent. These ashes have a potential effect in rising pH when dispersed in water; so, they can be used as solid activators in one-part MK- and fayalite slag- based geopolymers **(Peys et al., 2017; Hu et al., 2009; Buchwald et al., 2009; Seiffarth et al.,2013; Ruiz-Santaquiteria et al., 2013; Feng et al., 2012; Malakooti et al., 2014; Khorasanipour 2015; Paramguru et al., 2005; Hind et al., 1999; Pontikes and Angelopoulos 2013; Vangelatos et al., 2009; Tsakiridis et al.,**

2004; Jamieson et al., 2016; Nie et al., 2016; Zhang et al., 2016; Ke et al., 2015; Ye et al., 2016; Choo et al., 2016; Chandrasekhar et al., 2003; Della et al., 2002; Armesto et al., 2002; Hajimohammadi and van Deventer 2016; Sturm et al., 2016; Venkatanarayanan and Rangaraju 2013; Peys et al., 2016).

Chlorosilane production has resulted in the formation of silica residue, which has a beneficial use in one-part geopolymers, if it was activated by solid sodium aluminate **(Strum et al. 2016, Strum et al. 2015)**. The silica content in this residue is in the range of 84-89 wt.% accompanied by chloride content of 0.86-0.36 wt.% **(Strum et al., 2016; Strum et al., 2015; Gluth et al., 2013).**

As another potential amorphous silica source, geothermal silica usually represented as a precipitated in the surface of pipes at geothermal power plants **(Pambudi et al., 2015)**. Before utilizing geothermal silica in one-part geopolymer preparation, it was washed with the hot distilled water at liquid to solid ratio 10 followed by filtration and washed again. The washed geothermal silica has been dried, melt and finally mixed with solid sodium aluminate (**Hajimohammadi et al., 2008**). The pre treatment of geothermal silica before its utilization in one-part geopolymer synthesis is due to the removal of salt, yielding material with silica content of 96 wt.% (**Hajimohammadi et al., 2008)**. Silica fume or micro silica as a byproduct of silicon and ferrosilicon alloy production can also be used in the preparation of one-part geopolymer (**Ye et al., 2016; Strum et al., 2016; Strum et al.,2015)** . Silica fume is a finally dispersed amorphous silica with particle size less than 1μm (**Khan and Siddique 2011)** The incorporation of 20-25 wt.% silica fume was found to have a positive impact on the mechanical properties of red mud – based one-part geopolymer (**Ye et al., 2016)**.

In addition to the above-mentioned silica-rich and wastes, the solid sodium meta silicate can be used as a an activator in one-part geopolymer. Actually, the utilization of wastes in the synthesizing of one-part geopolymer mainly depends on their local availability.

2.9. Admixtures in one-part geopolymer

Superplasticizers were found to have high efficacy in workability rheology, and mechanical properties of conventional OPC mortar or concrete. Naphthalene, lignosulphonate, polycarboxylate, melamine-based compounds are the main superplasticizers. Nevertheless,

the most of superplasticizers showed a slight effect on the properties of geopolymer **(Shaikh 2013**).

A promising effect on the performance of two-part geopolymer was recorded in the case of naphthalin (**Hardjito et al., 2005; Palacios et al., 2008; Palacios and Puertas 2005; Hardjito et al., 2004; Palacios et al., 2009)** and modified polycarboxylates **(Nematollahi and Sanjayan 2014; Memon et al., 2012; Carabba et al., 2016)**. Sodium lignosulphonate with 0.5 wt. % has resulted in the enhancement of one-part red-mud-based geopolymer (**Ye et al., 2016)** as it was found to reduce water content by 18 % accompanied by compressive strength improvement. In another work, the addition of poly carboxylic acid based-superplasticizer has reduced water content of one-part alkali activated slag by 65 wt. % **(Yang et al., 2010)**.

One-part geopolymer was characterized by rapid setting as the result of heat released from activator dissolution such as solid NaOH **(Suwan and Fan 2017)**. Accordingly, retarders mixture should be added to slowdown one-part geopolymer setting. A significant effect on one-part geopolymer setting was recorded by the embedding nano-ZnO in geopolymeric structure. The reason behind retardation effect is the formation of calcium zincate phase which negatively affects the nucleation of calcium sodium aluminosilicate binding phase **(Garg and White 2017)**. Phosphoric acid (**Chang 2003**) and sodium phosphate (**Gong and Yang 2000**) were found to have a potential impact on the retardation of alkali activated slag setting by the formation of $CaHPO_4$ and $Ca(H_2PO_4)_2$ phases **(Kalina et al., 2016)**. Also, the high dosages of inorganic salts and sucrose have also been used as apotential retarders of alkali activated slag cement **(Brough et al., 2000)**. Tartaric acid and unspecified phosphate retarders were also found to have a significant impact on the rheology of geopolymeric materials **Van Deventer et al., (2010); Wang et al., (2017)**. The addition of 0.5 wt. % nano-sized Al_2O_3, ZnO, and ZrO_2 positively affects the compressive strength of one-part geopolymer **Hajimohammadi et al., (2011) .**

2.10. Properties of one-part geopolymers and their preparation strategies

Andrew (2017) have synthesized one-part alkali activated alumino silicate by the calcination of bentonite-dolomite blend in the presence of sodium carbonate (Na_2CO_3). The highest 28- days compressive strength (33.8 MPa) of 80°c cured sample was obtained by

the calcination of bentonite-dolomite with CaO & MgO /SiO_2 molar ratio of 2.1 and Na_2O/SiO_2 molar ratio of 0.4. This mix showed compressive strength twice higher than that of calcined bentonite – dolomite in the absence of Na_2CO_3. As proved by X Ray diffractograms (XRD). Thermally-treated material is mainly composed of amorphous phases with the formation of ill-crystalline C_3A, belite and MgO phases. The rising temperature up to 1200°C makes the MgO remained in thermally-treated mixture has low reactivity. The same trend was obtained in the absence of Na_2CO_3. Hydrated lime ($Ca(OH)_2$) was released during the hydration of belite in thermally treated mixture without alkali addition; Meanwhile this hydroxide not observed in thermally-treated alumino silicates with Na_2CO_3 addition. The exposure of the optimum mixture cured at 80°C to accelerated carbonation led to the formation of high compact microstructure. The addition of alkali during thermal treatment significantly improved the engineering properties of the prepared one-part alkali activated material.

Other workers have tried to create one-part geopolymer by mixing $NaAl_2O_3$ with different Si-rich-materials with or without GGBFS **Shenider et al., (2011)**. They have found that the resistivity of the prepared mortars enhanced with the increase of Si content in geopolymeric matrix; mean while a significant reduction in geopolymer mortar resistivity had been recorded by the increase of slag addition level. The main reason behind the dominant effect of Si increment in one-part geopolymer mortar was due to the formation of silica gel around binding materials which in turn acts as protective layer. The increase in slag content (as a good Ca source) resulted in acid resistivity reduction which caused by the formation of expensive phases such as $CaSO_4$.**Damtoft et al., (2008)** Prepared heat and ambient cured one-part geopolymeric materials by blending solid activators with low Ca FA, slag and hydrated lime composites. Three different Na –Si grades and a mixture of Na_2SiO_3 and NaOH powders has been used in the formation of one-part geopolymer. Type and amount of solid activator, FA replacement by slag and $Ca(OH)_2$, and water content were the main parameters which influenced on the workability of the fresh paste. density and compressive strength of hardened geopolymeric materials at ambient and heat cured conditions. The highest performance was observed in case of one-part geopolymers based on low Ca FA-hydrated lime – sodium silicate composite. The compressive strength of prepared one-part geopolymer increased with alkali activated content; whereas the highest compressive

strength of 37 MPa was recorded when alumino -silicate material activated by of 12 wt. % of Na_2SiO_3.

Flatt et al. (2012) have prepared one-part geopolymer cement by mixing slag with different contents (2, 4, 6, 8 and 10 wt. %) of NaOH and mixing water which makes the pastes in non-workable forms then dried and pulverized to produce powder with definite particles size. They are found that the hardened materials affected by (i) the increment of NaOH content, and (ii) the content of water/slag ratio at constant one of them. Comparing with two-part geopolymer cement, one-part mixture material showed the lower compressive strength at constant NaOH content. The prepared powder can react with water like PC, yielding hardened material with high compressive strength. The preparation of one-part alkali activated binders using ceramic waste and GGBFS was conducted by **Gartner and Hiaro (2015)** . Fiber type addition and curing condition were found to have a potential impact on microstructural development, producing hardened activated material with flexural strength in the range of 10 to 40 Mpa.

Abdel-Gawwad et al., (2018) have synthesized one-part alkali activated geopolymer by exposure ground air cooled slag at elevated temperature in the presence of alkali activator (NaOH) as a fluxing material), yielding alkali activated powder with high hydration property such as Portland cement. The Fourier transformer infra-red (FTIR) and X ray diffractograms (XRD) proved that as the content of NaOH increase; the amorphous structure increase. Meanwhile; **Provis (2017)** fabricated one-part geopolymer by thermal activation of red mud in the presence of alkali. Silica fume had been mixed with thermally treated sample to optimize geopolymer composition. The prepared one-part geopolymer can easily react with water like PC, resulted in hardened material with acceptable performance. They found that in the absence of silica fume the hardened one-part geopolymer demonstrated poor mechanical properties which related to the lower SiO_2/Al_2O_3 molar ratio. Therefore, silica fume was added to increase SiO_2/Al_2O_3 molar ratio. The highest 28 days compressive strength (31.5MPa) was recorded when SiO_2/Al_2O_3 molar ratio adjusted at 3.45 with mixing water of 45% (by weight of one- part geopolymer powder). The activation mechanism of one- part geopolymer was performed by the liberation of Na from aluminosilicate network and consequently activates SF, which participated in geopolymerization process.

Complementary, one-part based geopolymer by mixing rice husk ash (RHA) with sodium aluminate which achieved SiO_2/Al_2O_3 of 3.5 **(Aiken et al., 2017)**. After 1- day of curing; the prepared binder exhibited the highest performance with compressive strength of 30MPa as proved by X Ray diffractograms (XRD) and Fourier transformer infra-red (FTIR), RHA can react with sodium aluminate to product amorphous geopolymeric gel with no formation of crystalline phases. **Bakharev (2005)** have designed one-part mix alkali activated cement using FA as a good source of aluminosilicate material and red mud as alternative to conventional NaOH activator. The results showed that the rate of geopolymaerization process enhances with increasing red mud content. The experimental methods explained that the use of red mud as alkaline activator has a nearly impact of sodium hydroxide (NaOH) at constant Na_2O/SiO_2 molar ratio. **Kong and Sanjayan** (**2010)** Synthesized one-part alkali activated alumino silicate composites (SHGC) which hardened at room temperature by reference. Some factors had been used to develop of geopolymer production which can be beneficially used as a good alternative to Portland cement. The results proved that the prepared one-part cementitious material showed the best strain hardening behavior which associated with the tensile strength of 4.6MPa and tensile strain 4.2%.

As an innovative material, one-part geopolymer foam was prepared using glass fines as a substituent to fine sand **((Sarker et al., 2014)**. By comparing geopolymer foam with different aggregate (glass and sand) and geopolymer foam without aggregate (as a control sample); the sample with sand aggregate has higher density that of sample with glass aggregate. The results explained that strength of glass aggregate geopolymer foam has a high value that of sand aggregate geopolymer, so density in glass sample is lower and lighter than that of sand sample.

CHAPTER III

METHODOLOGY

3.1. Diagram Describing the Whole Project

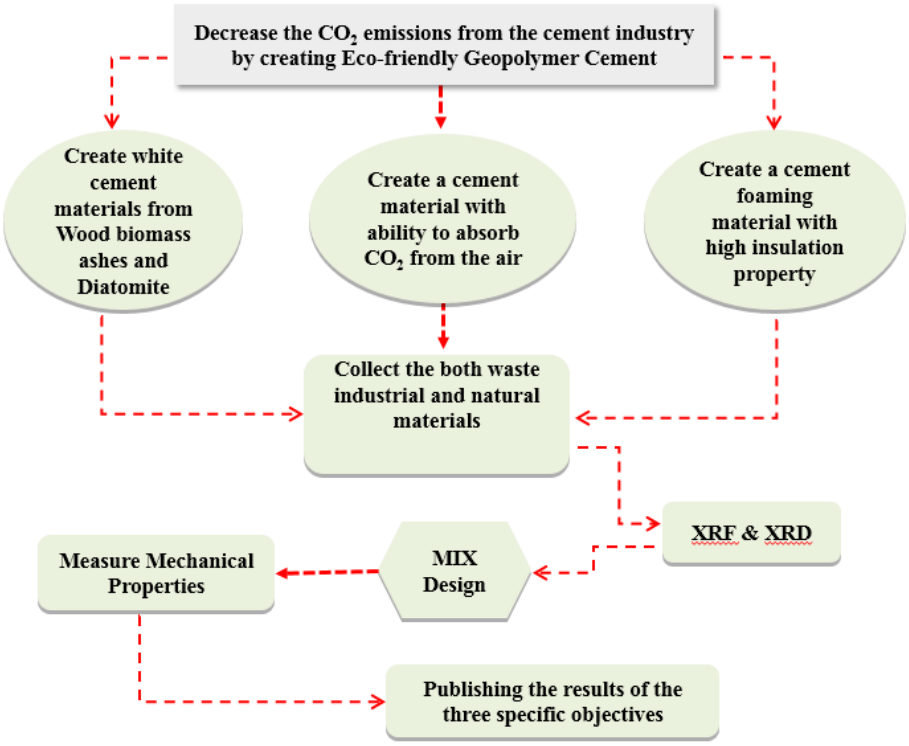

3.2. Materials

The main materials and chemicals utilized in the three specific objectives are Diatomite, wood biomass ash (WBA), and sodium hydroxide (NaOH) are the starting materials used in this investigation. Diatomite was brought from eastern side of Morelia city, Michoacán, Mexico. WBA was collected from local open yards clay bricks furnaces in Michoacán state, Mexico and NaOH with purity of 99.99% was purchased from Fisher Scientific Company, UK. The chemical compositions of WBA supplied from different eight-locations in Michoacán state Charo, Salamanca, Patzcuario, Urapan, Quiroga, Zentacuaro, Tarimbaro and Apatzingan are given in Table 1. Due to high calcium content in WBA-Charo, it was chosen in the preparation of dry activator. The chemical composition of diatomite is listed in Table 2.

Table 1: Means standard deviation and chemical oxide (wt. %) of WBA from different locations in Michoacán state, Mexico.

Oxides	SiO_2	Al_2O_3	Fe_2O_3	CaO	MgO	Na_2O	K_2O	SO_3	TiO_2	P_2O_5	Loss
WBA- Charo*	0..98	1.51	1.19	44.81	3.81	1.64	6.89	1.07	0.288	1.72	35.90
WBA-Salamanca	2.3	1.41	1.75	43.38	2.91	2.46	4.8	3.48	0.87	2.35	34.06
WBA-Patzcuario	4.4	2.34	2.59	40.85	2.56	1.22	7.17	5.54	0.33	2.32	30.64
WBA-Urapan	5.54	2.93	2.54	37.68	3.95	4.04	6.45	3.33	0.43	3.44	29.6
WBA-Quiroga	6.53	2.39	2.67	35.32	5.98	3.75	7.54	3.56	0.98	3.4	27.68
WBA-Zentacuaro	4.44	1.54	1.95	41.65	1.65	6.54	6.56	1.1	0.28	2.54	31.56
WBA-Tarimbaro	21.86	7.29	2.56	29.36	2.55	2.54	3.89	4.76	0.97	1.65	22.51
WBA-Apatzingan	19.65	8.21	2.98	27.98	3.82	1.43	5.68	2.28	0.89	5.67	21.39
Standard deviation	7.96	2.72	0.59	6.45	1.31	1.78	1.25	1.60	0.32	1.31	5.13

* Means that the WBA-Charo was used as calcium-rich source in the preparation of one-part geopolymer

Table 2: Chemical composition of Diatomite.

Oxides	SiO_2	Al_2O_3	Fe_2O_3	CaO	MgO	Na_2O	K_2O	SO_3	TiO_2	P_2O_5	Loss
Diatomite	80.3	6.1	6.79	1.04	0.65	0.62	0.44	0.12	0.67	0.79	2.30

The other raw materials are, Coconut ashes (CA) and aluminum slag AS are derived from huge waste reserves in Charo, village 10Km west of Morelia city, Michoacán, México. It produced from the burning of coconut shells which used as alternative fuel in fabrication of brick stones. AS was supplied from from Almexa, Toluca state, Mexico. The chemical compositions of CA and AS are listed in Table 3, using X-ray fluorescence (Philips X'Pert PRO MPD spectrometer).

Table3. Chemical compositions of CA and AS.

Oxide, %	*SiO_2*	*Al_2O_3*	*Fe_2O_3*	*CaO*	*MgO*	*Na_2O*	*K_2O*	*SO_3*	*Cl-*
CA	24.6	10.3	8.84	30.8	6.53	0.62	17	0.526	0.7
AS	21.42	72.37	1.03	4.30	0.95	0.32	0.15	0.06	0.04

Finally, two types of naturally occurring volcanic ashes (namely, white and red volcanic ashes) and reactive magnesium oxide (MgO) are the main raw materials used in the fabrication of CO2-capture materials. White and red volcanic ashes (WVA and RVA) were

obtained from, a field area close to Morelia city, Michoacán state, Mexico; meanwhile, MgO was purchased from Fisher Scientific Chemical Company (UK). The chemical compositions, which were conducted by X-ray fluorescence (XRF: Xios PW1400), and physical properties of volcanic ashes and MgO are reported in Table 4.

Table4: Chemical compositions and physical properties of starting materials.

Mixtures notations	**Chemical compositions, wt. %**									**Physical properties**		
	SiO_2	CaO	MgO	Fe_2O_3	Al_2O_3	Na_2O	K_2O	P_2O_5	TiO_2	Specific gravity	Amorphous content	Color
WVA	71.30	2.39	0.45	4.60	13.10	1.17	5.01	0.91	0.83	2.65	72	White
RVA	47.32	10.81	2.32	15.61	15.30	2.30	1.84	1.29	2.52	2.83	39	Red
MgO	-	-	99.57	-	-	-	-	-	-	1.92	-	White

3.3. Geopolymer Synthesis

In the following lines it will describe the techniques and characterizations of each specific objective's individual.

3.3.1. Cleaner production of one-part white geopolymer cement using pre-treated wood biomass ash and diatomite

The X-ray diffractograms (XRD) demonstrated that the diatomite is mainly composed of amorphous aluminosilicate structure with a hump at 5-40 2θº **(See Fig. 1).** As estimated by the Rietveld analysis of XRD, diatomite mainly possesses 85% amorphous content. Meanwhile WBA represented different crystalline peaks affiliated to $CaCO_3$. Diatomite was chosen in this study because of its white color which when blended with pretreated calcium-rich WBA yields one-part white geopolymer cement.

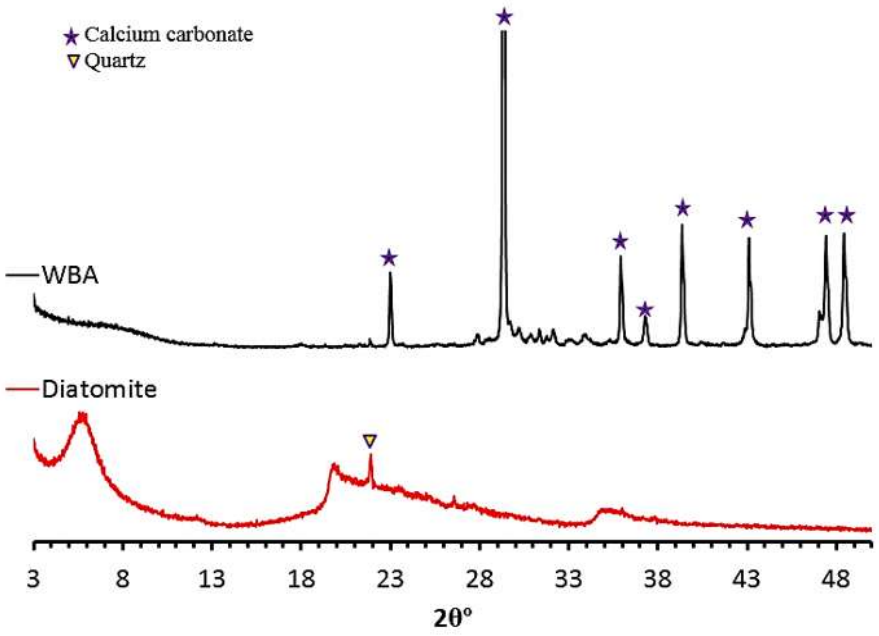

Fig. 1: XRD-patterns of wood biomass ash (WBA) and diatomite.

Table 5 shows the mix proportions of dry activator (DA). As proved from chemical analysis, WBA is mainly composed of ~80% $CaCO_3$. It was treated by NaOH at different NaOH: $CaCO_3$ molar ratios of 2, 1, 0.5, and 0.25 at water to WBA (W/WBA) ratios of 0.45, followed by drying at 80ºC for 24h. The solidified materials were pulverized for 30 sec. using ball mill Machin to pass through 75µm sieve, yielding DA, which mainly composed of natrite (Na_2CO_3), calcium hydroxide {$Ca(OH)_2$} pirssonite {$Na_2Ca(CO_3)_2.2H_2O$} and unreacted $CaCO_3$. The XRD-patterns **(Fig. 2)** proved that the amount of unreacted $CaCO_3$ and pirssonite decreased with the increase of NaOH/$CaCO_3$ molar ratio. Where, the pattern corresponding to WBA, which treated by 2 mole of NaOH (DA1) found to be fully composed of $Ca(OH)_2$ and Na_2CO_3 with no observation of $Na_2Ca(CO_3)_2.2H_2O$ and $CaCO_3$. This is associated with the enhancement of cationic exchange reaction of Na/Ca with the increase of NaOH content.

$$\mathbf{2NaOH + CaCO_3 \rightarrow Ca(OH)_2 + Na_2CO_3}$$

Gibbs equation ($\Delta G = \Delta H - T\Delta S$) was applied to confirm that the reaction between sodium hydroxide and calcium carbonate is spontaneous reaction at 25ºC (298 kelvin). By applying the calculated enthalpy (ΔH = -58.24 kJ/mole) and entropy (ΔS = 0.00469 kJ/mole) at

temperature (T) of 298 kelvin, a negative value (-59.63 kJ/mole) was recorded. Where this value is an indication of the spontaneously of this reaction.

Table 5: Mix proportions of dry activators.

Dry activator notations	NaOH (g)	WBA (g)	NaOH/$CaCO_3$ molar ratio	NaOH wt., %
DA1	64	100	2.0	39
DA2	64	200	1.0	24
DA3	64	400	0.5	14
DA4	64	800	0.25	7

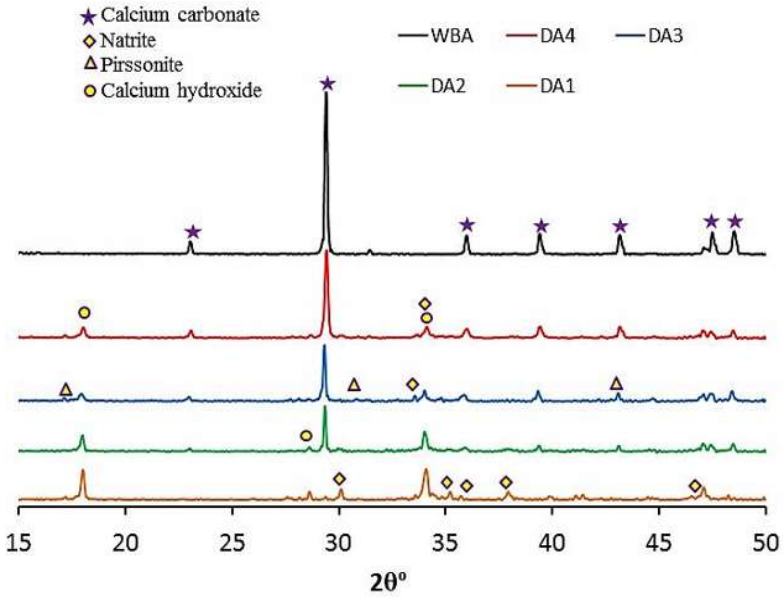

Fig. 2: XRD-patterns of wood biomass ash (WBA) and dry activators (DAs).

For One-part geopolymer preparation, diatomite was crushed to pass from 75µm sieve. The particle sizes distribution **(Fig. 3)** proved that there is no significant variation in mode size of dry activator and diatomite. Different DA contents were individually added and carefully mixed with diatomite powder to ensure complete homogeneity. All DAs added to diatomite were calculated to achieve 3 wt. % of NaOH in each mix. Where the amount of DA increased with decreasing NaOH/$CaCO_3$ molar ratio. After complete dry mixing of diatomite and WBA, the water has been added to the prepared one-part white geopolymer cement (WGPC) to form a workable paste. The Vicat test proved that all blends require the same water content to achieve the standard consistency. After wet mixing, the workable

paste was transferred to stainless steel mold of 5×5×5 cm^3, followed by curing in 99±1% relative humidity (RH) for 24h at 23±2ºC. The hardened cubes were demolded and cured at the same conditions until testing. The details of mixing proportions of the investigated mixes are given in **Table 6.** The life cycle of one-part white geopolymer cement is shown in **Fig. 4**.

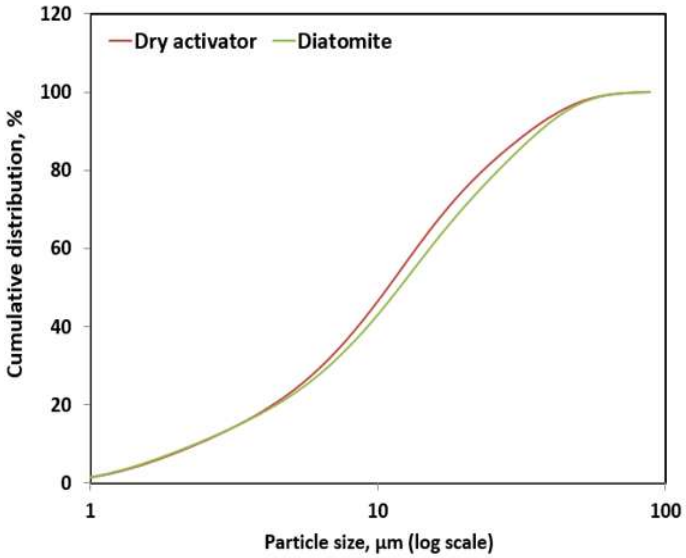

Fig. 3: Particle size distribution of diatomite and DA.

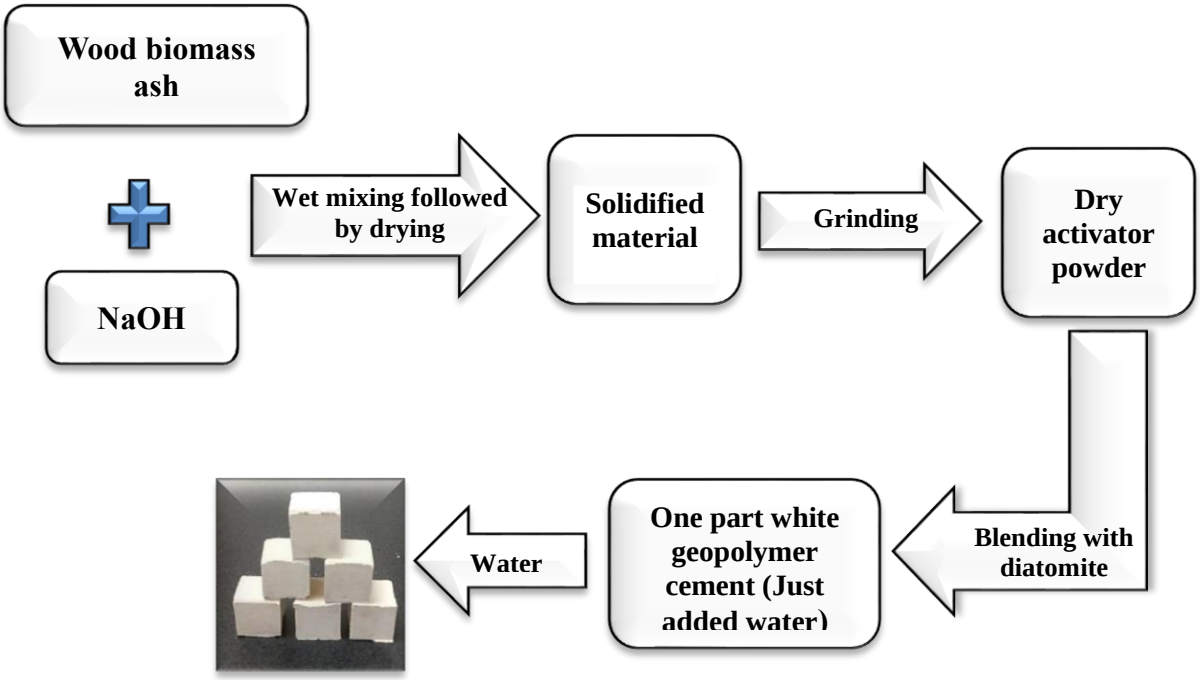

Fig. 4: Life cycle of one-part white geopolymer cement production.

Table 6. Proportions of the investigated one-part WGPCs.

GPC-notations	DA, %	Diatomite,%	W/P ratio	NaOH equivalent, wt.%
WGPC-DA1	7.70	100	0.27	3
WGPC-DA2	12.5	100	0.27	3
WGPC-DA3	21.5	100	0.27	3
WGPC-DA4	43.0	100	0.27	3

Setting times of the prepared one-part WGPCs were measured using Vicat apparatus according to ASTM C191 (2013). Compressive strength testing was conducted on 3-hardened cement cubes according to ASTM C109M (2016) using five tons German-Bruf-Pressing Machine with a load capacity of 175kN. After compressive strength testing the hydration reaction of WPGC was stopped by immersing broken samples in methanol and acetone, at volumetric ratio of 1:1, for 24h followed by drying at 80ºC for the same time and kept in tightly contact vessel until analyses. The total porosity percentages of the hardened specimens were detected using mercury intrusion data from an Auto Pore IV 9500 porosimeter. The whiteness of one-part WGPC powder was measured by color measurement apparatus, (Model color Flex EZ).

XRD-analysis was conducted using Philips PW3050/60 diffractometer with a scanning range from 5 to 50(2θ), and a scanning speed of 1s/step as well as resolution of 0.05°/step. The Fourier transform infrared (FTIR) spectroscopy was carried out using KBr discussing Genesis-IIFT-IR spectrometer in the range of 400-4000 cm^{-1}. TGA/DTG were performed by heating of ~50mg of specimens powder in nitrogen atmosphere up to 1000 °C at a heating rate of 10 °C/min using a DT-50 Thermal Analyzer (Schimadzu Co-Kyoto, Japan).

3.3.2. The potential application of eco-friendly magnesia-silicate cement in CO_2 sequestration

The chemical analyses of the starting materials prove that the White volcanic ash WVA and Red volcanic ash RVA are mainly aluminosilicate materials. X-ray diffraction (XRD) **(Fig. 5)** proves that, the pattern of WVA represents a hump at 2θ range of 15-30º with the

appearance of well-resolved sharp peaks affiliated to crystalline phases such as albite, and margarita minerals. This hump is an indication of the amorphous nature of WVA. The RVA demonstrates crystalline thenardite, margarita, and wavelite peaks with no appearance of an amorphous hump, indicating the low amorphicity content in RVA. The quantitative Rietveld XRD-analysis shows that, the WVA demonstrates amorphicity content of 72% higher than that identified in the case of RVA (39%).

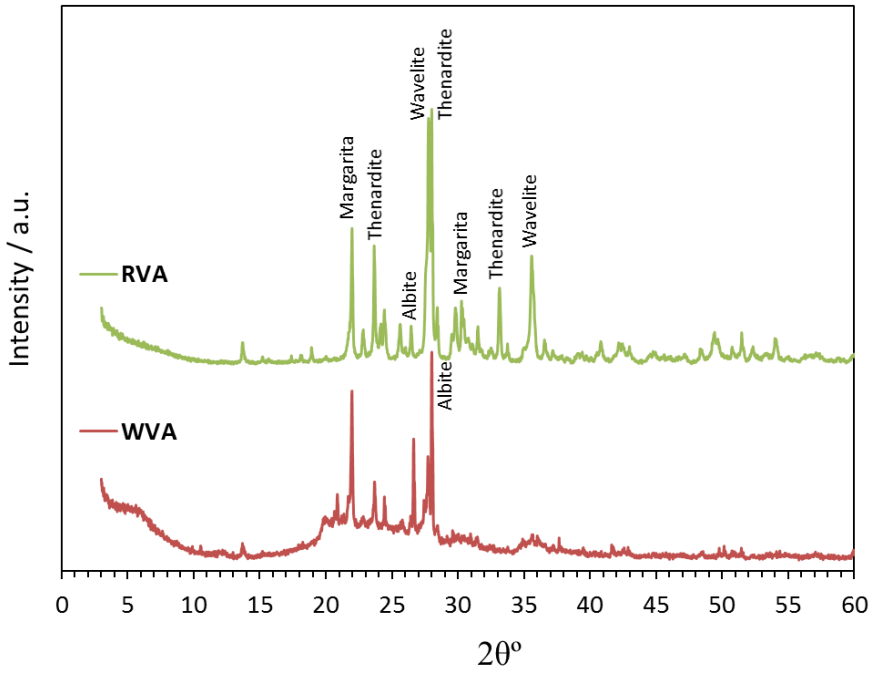

Fig. 5. XRD-patterns of white and red volcanic ashes (WVA and RVA).

3.3.2.1. Fabrication of CO_2-capture materials

Flow chart of the preparation steps including hydration and carbonation curing is represented in **Fig. 6**. Firstly, WVA and RVA are ground to pass through 100 µm sieve followed by dry mixing with MgO for 5 min, using ball mill machine. Volcanic ashes-MgO blends were designed at weight ratio of 1:3. The MgO was used with high content in cement blend to offer favorable conditions for accelerated carbonation. After formulation step, mixing water (at water to solid ratio of 0.40) was added to homogenous dry WVA-MgO and RVA-MgO mixes, yielding workable pastes. The details of mixing proportions are reported in **Table 7.** The fresh pastes were transferred to stainless steel molds of 50 x 5 x 50 mm, followed by curing in humidity chamber with 99±1% relative humidity (RH) at

23±2ºC. After 24h of curing, the hardened cubes were demolded and cured at the same conditions for 28-days to achieve considerable compressive strength.

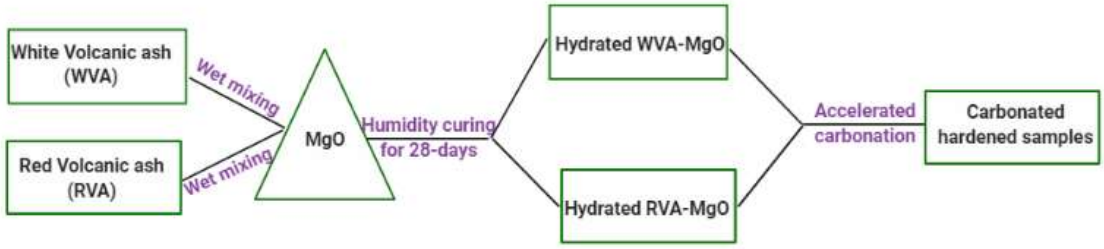

Fig. 6. Basic diagram of the preperation, hydration, and carbonation processes.

Table7. Mixing proportions of magnesium silicate-based cement.

Mixture notation	WVA	RVA	MgO	W/P ratio
	wt. %			
WVA-MgO	25	-	75	0.40
RVA-MgO	-	25	75	0.40

The 28-days cured samples (zero time of carbonation) were transferred to stainless steel CO2-champer with RH of 75%. To ensure the medium with 100% CO2 environment before conducting accelerated carbonation test, the open chamber was flashed with CO2 for 2 min. After CO2-flushing, the top outlet of the chamber was closed to proceed the accelerated carbonation of the hardened materials. The CO2-pressure adjusted at 20 atm. using dial gauge contented to CO2 cylinder. At different time intervals such as 1, 14, and 28-days, the carbonated samples were taken out and kept for 24h at 50±5 % RH and 23±2ºC before conducting strength measurements and solid phase identification using XRD, thermo-gravimetric (TG/DTG) analysis, and Fourier transform infrared (FTIR) spectroscopy.

3.3.2.2. Experimental methods

Compressive strength testing was carried out on the hardened cubes following the procedure described by (C109M, 2016). The compressive strength value was taken as an average of 5-specimen readings. In order to remove irregularities, the surface of the specimen was carefully polished by filter paper. Compressive strength measurements were carried out using five tones German Brüf Pressing Machine with a maximum load capacity of 175kN. Mercury intrusion data from an Auto Pore IV 9500 porosimeter was applied to determine the change in the total porosity of the hardened materials before and after carbonation reaction.

3.3.2.3. Phase identifications

XRD-analysis was used to determine the crystalline phases in the cured and carbonated samples using Philips PW3050/60 diffractometer with 5 to 60 (2θº) scanning range, 1s/step scanning speed, and 0.05°/step resolution. All the obtained peaks were identified according to powder diffraction file (PDF). A DT-50-Thermal Analyzer (Schimadzu Co-Kyoto, Japan), which provided by cryostat for cooling process, was used to perform the TGA of carbonated and cured samples. The weight percentage of CO_2-sequestrated (CO_2 wt. %) by the hardened samples during CO_2-exposure was calculated by dividing the weight loss of $MgCO_3$-phase (WL) by the total weight loss (TWL) of sample as follow:

$$CO2, wt.\% = \frac{WL}{TWL} * 100$$

FTIR-analysis was carried out on some selected samples in order to identify the functional groups of hydration products via KBr discussing Genesis-IIFT-IR spectrometer at the wavenumber range of 400-4000 cm^{-1}.

3.3.3. The creation of a geopolymer foam with high thermal insulation properties from Coconut ashes wastes

The X-ray diffractograms proved the amorphous structure of coconut ash CA having crystalline peaks related to quartz, lime, calcite and preicalse **(Fig.7a)**. The AS is mainly composed of different crystalline peaks affiliated to spinel, crystoballite, corundum, bixobite and alumina metal **(Fig.7b)**. The rietveld x-ray diffraction proved that the AS contains 7% of Al metal. Before alkali activation of CA, it milled to pass from 45µm sieve

to remove any contaminants. Also, AS has been crushed and passed from the same sieve size.

Unfoamed geopolymeric materials was synthesized by alkali activation of CA. It activated by 4, 5 and 6 % NaOH (with respect to CA-powder). After mixing of CA with alkaline solution, the slurry was transferred to one-inch cubic steel mold and cured for 24h in 99±1% relative humidity (RH).

For foamed geopolymeric materials, different AS contents (3, 5 and 7 %) were carefully dry-mixed with CA-powder; followed by mixing with alkaline solution. Three W/CA ratios were applied in the preparation of CA-based geopolymer foams i.e. 0.30, 0.35 and 0.40.

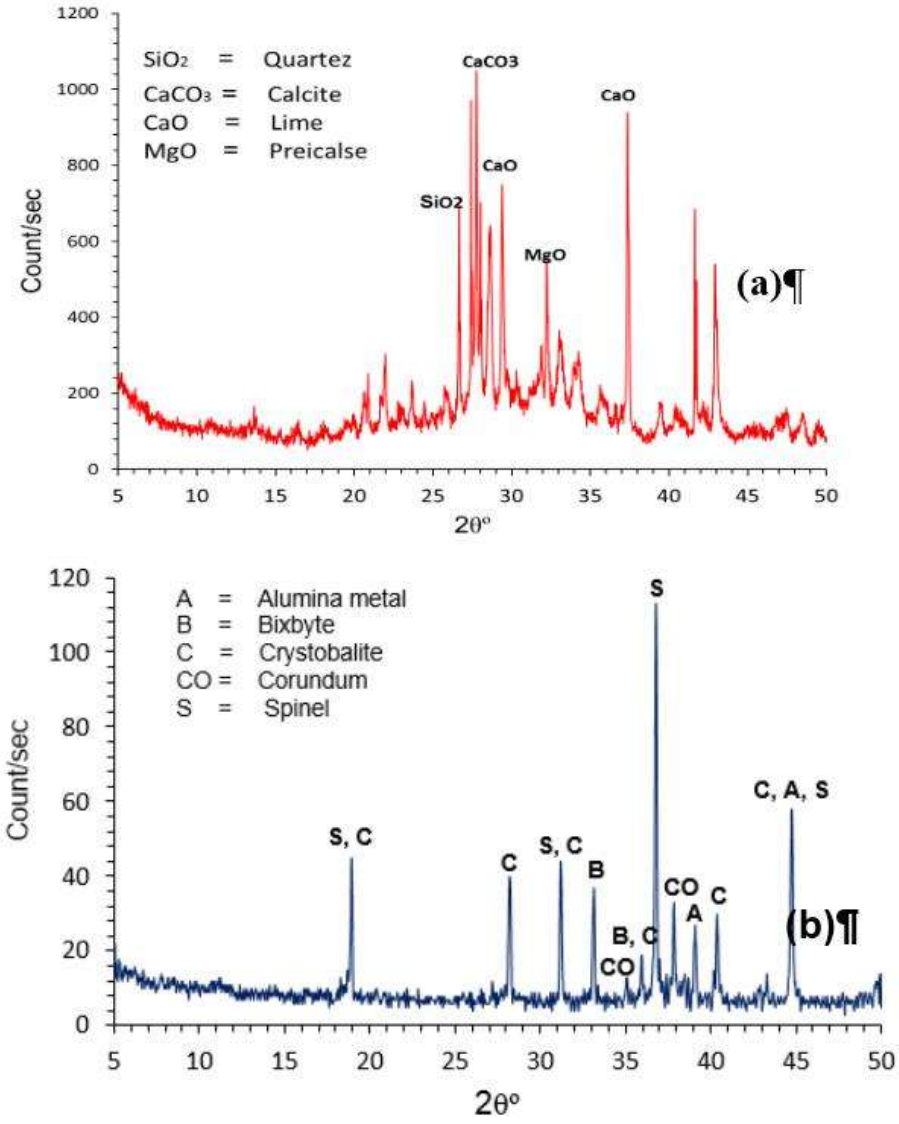

Fig. 7: XRD-patterns of (a) coconut ash and (b) alumina slag.

The details of mix proportions are given in **Table 8**. After complete mixing, the workable paste was transferred to one-inch cubic mold and cured in 99±1% RH for 24h. The hardened foamed and unfoamed CA-based geopolymeric materials were demolded and cured under the same condition for 28-days.

Table 8. Mix proportions (mass, %) of foamed and unfoamed geopolymeric materials

Mix notations	***CA***	***NaOH***	***AS***	***W/CP***
CA-4	100	4	-	0.30
CA-5	100	5	-	0.30
CA-6	100	6	-	0.30
CA-5/AS3	100	5	3	0.30
CA-5/AS5	100	5	5	0.30
CA-5/AS7	100	5	7	0.30
CA-5/AS7-1	100	5	7	0.35
CA-5/AS7-2	100	5	7	0.40

The compressive strength test was carried out on three samples according to ASTM C109M-16 specification (C109M) using five tons German-Bruf-Pressing Machine with a loading rate of 100kg/min. Thermal conductivity was measured with a thermal conductivity analyzer (Applied Precision ISOMET 2104). The bulk density and total porosity of the geopolymer foam were measured using the Archimedes method in deionized water.

3.4. Characterization Techniques used for preparing the proposed different geopolymers.

3.4.1. XRD Analysis

XRD-analysis was conducted using Philips PW3050/60 diffractometer with a scanning range from 5 to 50(2θ), and a scanning speed of 1s/step as well as resolution of 0.05°/step.

3.4.2. FTIR Spectroscopy

The Fourier transform infrared (FTIR) spectroscopy was carried out using KBr discussing Genesis-IIFT-IR spectrometer in the range of 400-4000 cm-1.

3.4.3. Thermogravimetric analysis and Difference Thermogravimetry Rations (TG/DTG)

TGA/DTG were performed by heating of ~50mg of specimens' powder in nitrogen atmosphere up to 1000 °C at a heating rate of 10 °C/min using a DT-50 Thermal Analyzer (Schimadzu Co-Kyoto, Japan).

3.4.4. SEM and EDS Compositional Analysis of the Samples Analysis

The scanning electron microscopy / energy dispersive X-Ray spectroscopy (SEM/EDS) for the different kinds of geopolymer samples were done by the Hitachi S-5200 SEM with slow scan mode, 10 kV accelerating voltage and 0-0.3mm working distance. Also, with different magnifications ranging from × 10.000 to ×100.000.

3.4.5. Total porosity

The total porosity percentages of measured different hardened specimens geopolymers were detected using mercury intrusion data from an Auto Pore IV 9500 porosimeter.

3.4.6. The Compressive Strength Testing

Setting times of the prepared one-part Geopolymers were measured using Vicat apparatus according to **ASTM C191 (2013)**. Compressive strength testing was conducted on 3-hardened cement cubes according to **ASTM C109M (2016)** using five tons German-Bruf-Pressing Machine with a load capacity of 175kN. In another occasions the The compressive strength test was carried out on three samples according to ASTM C109M-16 specification (C109M) using five tons German-Bruf-Pressing Machine with a loading rate of 100kg/min.

CHAPTER IV

RESULT AND DISCUSSIONS

In the following paragraph we will integrated as much as we can all the three specific objectives together.

4.4.1. Cleaner production of one-part white geopolymer cement using pre-treated wood biomass ash and diatomite

A. Setting times

As one of the main physical requirements of cements, initial and final setting times (IST and FST, respectively) were conducted on all one-part WGPCs as given in **Fig. 8.** The increase in dry activator content up to 21.5 wt. % (WGPC-DA3) led to shorten IST and FST of WGPC. This may be due to the nucleating site impact caused by calcium carbonate in pre-treated WBA. Similar observation was reported by **Abdel-Gawwad and Abo El-Enein (2016); Camiletti et al. (2013),** which stated the presence of desirable calcium carbonate content in cement matrix can accelerate the formation of hydration products. The WGPC-DA4 showed the longest setting times, confirming the fact that calcium carbonate causes the dilution of amorphous silicate content which negatively affects the formation of binding-giving-phases **(Yip et al., 2008a)**. From previous outcomes, the setting times of WPGC-DA1, WPGC-DA2 and WPGC-DA3 are located within the range of **ASTM C150M (2013)** which stated that the initial setting time should be not shorter than 45 and final setting time not exceed than 375 min. This proved that the prepared cement can be beneficially used in concrete making.

B. Total porosity

The total porosity percentages of all hardened one-part WGPCs pastes up to 56-days of curing are graphically represented in **Fig. 9.** Clearly, the total porosity of all hardened cement deceases with curing time, confirming the formation of hydration products was on going with time. The total porosity varied from ~15 to ~24% at 56-days, depending on the amount of dry activator content. The positive filling effect of $CaCO_3$ on total porosity reduction of one-part WGPCs has been demonstrated in case of WGPC-DA2 and WGPC-

DA3. Where, the lowest total porosity was detected in case of WGPC-DA3, agreeing with the finding obtained by **Adesanya et al., (2018) and Ghosh (2017),** which stated the capability of the appropriate $CaCO_3$ content in the reduction of pore size of the hydrated cement. A significant increase in total porosity was observed in case of WGPC-DA4. This could be explained by the formation of limited amount of reaction products caused by the increase of $CaCO_3$ on the expense of amorphous aluminosilicate content **(Yip et al. 2008).**

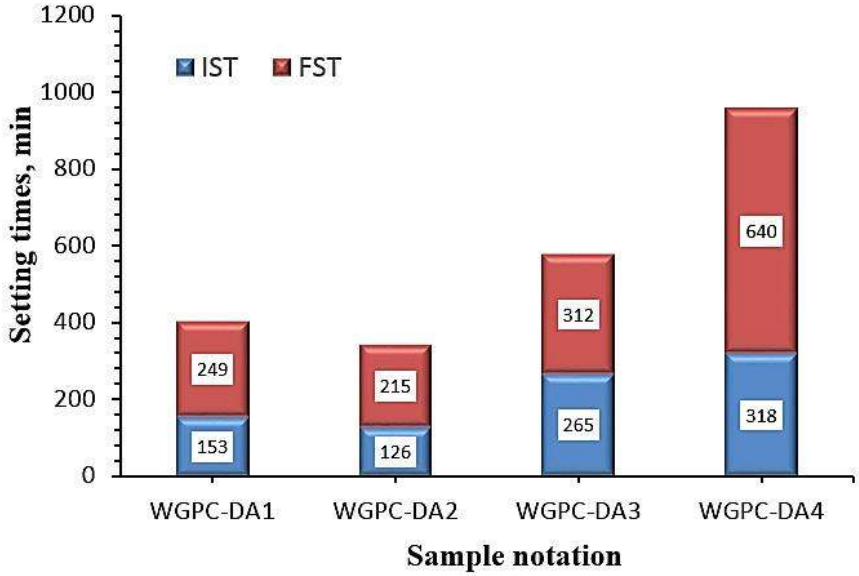

Fig. 8: Setting times of the prepared one-part white geopolymer cements.

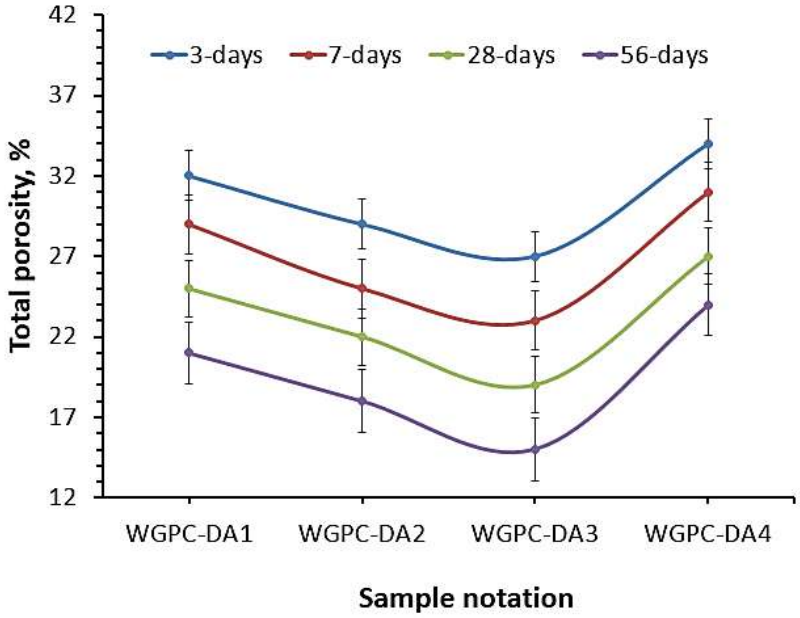

Fig. 9: Total porosity% of the hardened one-part white geopolymer cements.

C. Compressive strength

The compressive strengths of the hardened one-part WGPCs are shown in **Fig.10.** Undoubtedly, the development of compressive strength of hardened one-part WGPC pastes with curing time is an indication of the efficacy of DA on the formation of strength-giving-phases. Where, the $Ca(OH)_2$ and Na_2CO_3, in DA, increase the pH of the medium which in turn have a potential impact on the dissolution of aluminosilicate network in diatomite, leading to the formation of AlO_4^{5-} and SiO_4^{4-} activated species. These species condensed with each other to yield silicate/alumiosilicate binder such as calcium silicate hydrate (CSH) and calcium aluminum silicate hydrate (CASH) **(Abdel-Gawwad et al., 2016; Davidovits, 2015)**. The WGPC-DA3 demonstrated compressive strengths of 48 and 53MPa at 28- and 56-days, respectively which are higher than those achieved by all other hardened WGPC-samples. In contrast, the WGPC-DA4 showed the lowest strengths at all curing ages of hydration. These variations in compressive strength values demonstrated the effect of $CaCO_3$-content, in DAs, on the performance of one-part WGPC. The maximum compressive strength achieved by WGPC-DA3 may be due to the nucleating site and filling effects of $CaCO_3$ in DA. **Yip et al. (2008a)** stated that the surface interaction between $CaCO_3$ and geopolymeric binder is the main reason for compressive strength enhancement. The poor strengths obtained by WGPC-DA4 could be attributed to a significant disruption of geopolymeric gel network which resulted from the reduction of aluminosilicate content.

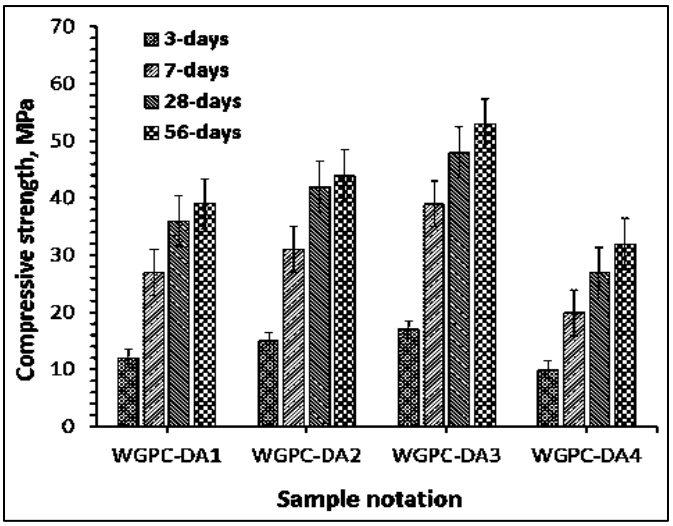

Fig. 10: Compressive strengths of the hardened one-part white geopolymer cements**.**

D. Whiteness of one-part WGPCs

The effect of pretreated WBA content on the whiteness of the prepared one-part WGPC is illustrated in **Fig. 11.** It is clear that the pretreated WBA has a negative impact on the whiteness of WGPC. The whiteness of 90, 88, 85, and 79% were recorded in case of WGPC-DA1, WGPC-DA2, WGPC-DA3 and WGPC-DA4, respectively. The possible explanation of whiteness loss is the presence of carbon in WBA, which resulted from the incomplete volatilization of carbon containing materials during burning of trees and coconut wood. Comparing ordinary white Portland cement (WPC), the WGPC-DA1 and WGPC-DA2 showed the highest whiteness; meanwhile WGPC-DA3 and WGPC-DA4 demonstrated the lowest values.

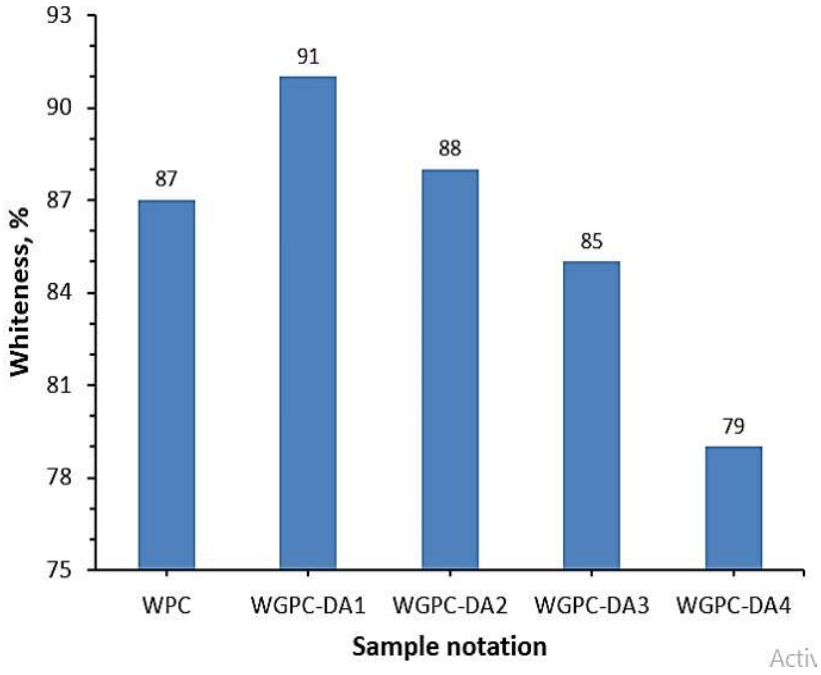

Fig. 11: Whiteness% of one-part white geopolymer cements.

E. Phases identifications

The x-ray diffractograms of one-part WGPCs at 28-days of hydration are stacked in **Fig.12.** All samples showed typical vitreous structure with crystalline $CaCO_3$ peaks, appeared at 2θ of 29.45º. The intensity of $CaCO_3$ peaks mainly depends on the DA -composition

(Adesanya et al., 2018). $CaCO_3$-peaks cannot be detected within XRD-pattern of WGPC-DA1, proving the fact that $CaCO_3$ was transformed to Na_2CO_3 and $Ca(OH)_2$ during treatment of WBA with NaOH at NaOH/$CaCO_3$ molar ratio of 2 **(See Table 5 and Fig. 2).** The WGPC-DA4 showed the highest $CaCO_3$-peak intensity, illustrating the presence of high $CaCO_3$ content in DA4 which obtained by treating WBA at NaOH/$CaCO_3$ molar ratio of 0.25. There are no distinct CSH or CASH peaks within all patterns, highlighting their amorphous structure **(Yip et al., 2008b)**.

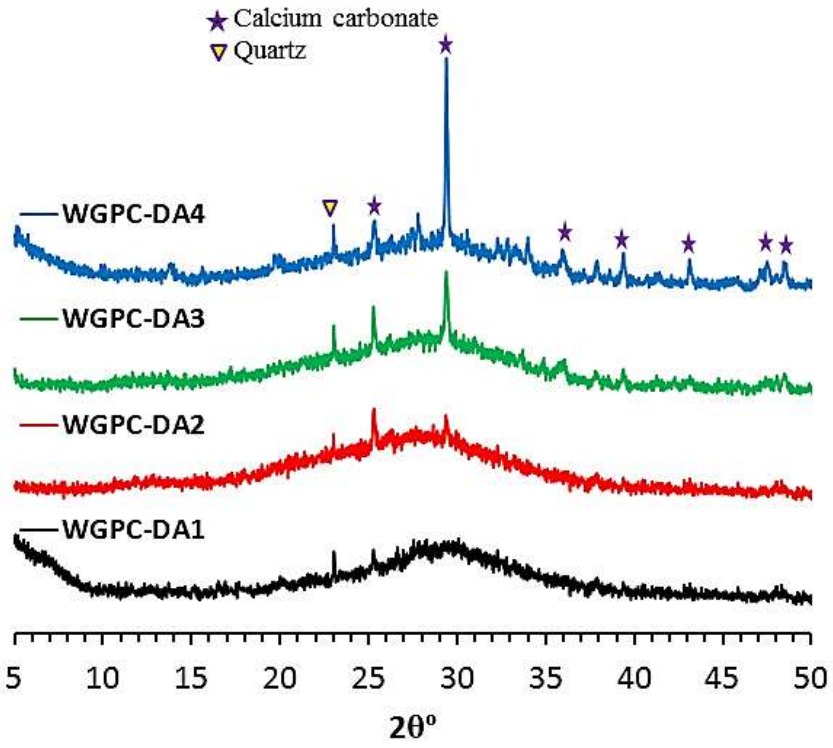

Fig.12: XRD-patterns of the hardened one-part white geopolymer cements.

The TG/DTG-thermograms of one-part WGPC samples at 28-days of curing are depicts in **Fig. 13.** Obviously, the weight loss related to the dehydration of free, physically adsorbed and combined water within CSH and CASH are detected at temperature range of 50-300°C. Meanwhile, the weight losses recorded at temperature 600-800°C are mainly due to the calcination of $CaCO_3$ originated from DA and atmospheric carbonation of WGPC. Although all samples activated by 3wt. %, there are differences in weight loss percentages and endothermic peak intensities among all one-part WGPC mixes. As shown in TG/DTG-curves, the WGPC-DA3 showed the highest weight loss as well as the highest CSH- and

CASH peaks intensity. This confirms the high efficacy of DA3 in the acceleration of hydration products formation in geopolymeric samples, complying with strength results. The lowest CSH and CASH as well as the highest $CaCO_3$-peaks intensity were obtained by WGPC-DA4. This proves the dilution of reactive aluminosilicate caused by the addition of high DA content.

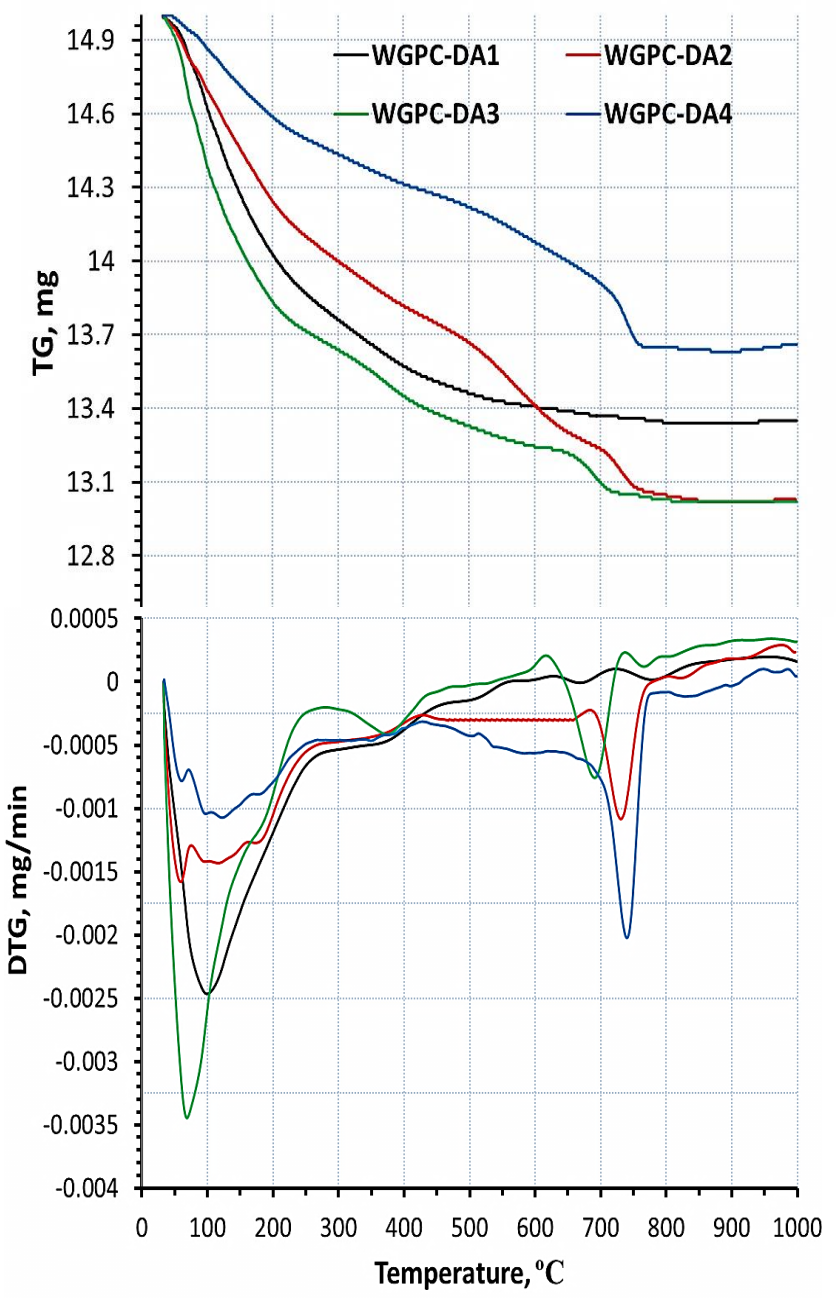

Fig.13: TG/DTG-curves of the hardened one-part white geopolymer cements.

Fig. 14 shows the relationship between the weight losses of CSH- and CASH-phases, and compressive strength values of all one-part WGPCs at 28-days of curing. Clearly, a direct relationship between CSH&CASH weight losses and strength values have been recorded with correlation coefficient (R2) of 0.99. The higher the CSH and CASH weight losses, the higher the compressive strength values. The addition of pretreated WBA powder up to 21.5wt. % leads to the increase of CSH and CASH content. This may be explained by the nucleating site impact of $CaCO_3$ (in DA) in the acceleration of hydration products formation. A further increase in DA content up to 43wt. % significantly reduces the aluminosilicate content which resulted in the retardation of CSH and CASH-formation.

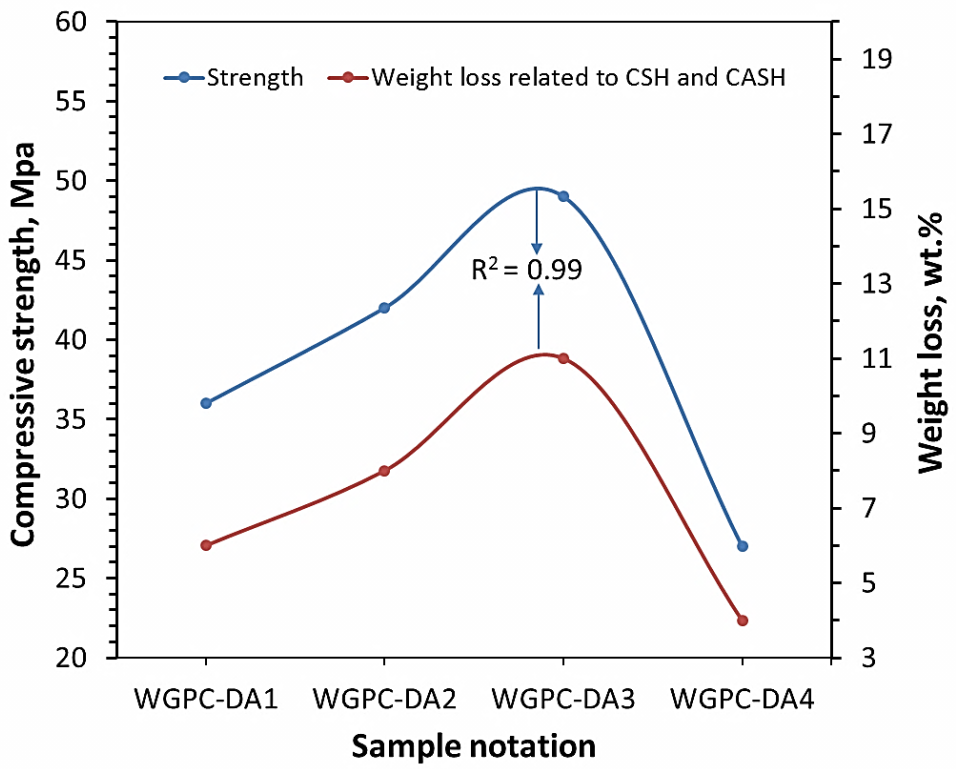

Fig. 14: Relationship between strengths and weight losses of CSH and CASH-phases.

The FTIR-spectra of diatomite and hardened WGPC-samples at 28-days of curing are stacked in **Fig. 15.** The FTIR-spectra exhibit different absorption bands. The bands appeared at 468-486 cm^{-1} are affiliated to bending vibration of Si-O-Si. Bands detected at 955-997cm^{-1} are mainly associated with stretching vibration of Si-O-Si(Al). Other bands affiliated to stretching vibration of OH and bending vibration of HOH within CSH and CASH were observed at 3458 and 1642cm^{-1}, respectively (**Mozgawa and Deja, 2009)**.

Well resolved absorption bands located at 1453 and 876cm^{-1}, are mainly related stretching vibration of carbonate containing phases. Evidently, a remarkable decrease in high full width at half maximum (FWHM) distance of Si-O-Si(Al) bands and significant increase in HOH and OH bands intensities were demonstrated after activation of diatomite by DA. These observations give a strong evidence on the effectiveness of DA in the dissolution of aluminosilicate network in diatomite to yield hydration products with high binding capacity and high ordering. Where, the reduction in FWHM distance means that the crystallinity and ordering of aluminosilicate network have been enhanced. Comparing with all spectra, the WGPC-DA3-spectrum showed the highest HOH and OH (within CSH and CASH) bands intensity as well as the smallest FWHM distance of Si-O-Si(Al) band. This confirms the fact that the desirable $CaCO_3$ content in DA3 acts as a nucleating site for growing hydration products, accelerating its formation rate. The GPC-DA4 exhibited the highest CO_3^{2-} bands intensity, suggesting the high $CaCO_3$ content in this mix. The highest Si-O-Si(Al) band broadness and the lowest HOH and OH bands intensity have been observed at the same mix, indicating the impact of high $CaCO_3$ content in the retardation of hydration products formation caused by the dilution of amorphous silicate content. The FTIR-spectra are in a good harmony with TG/DTG, XRD, and compressive strength results.

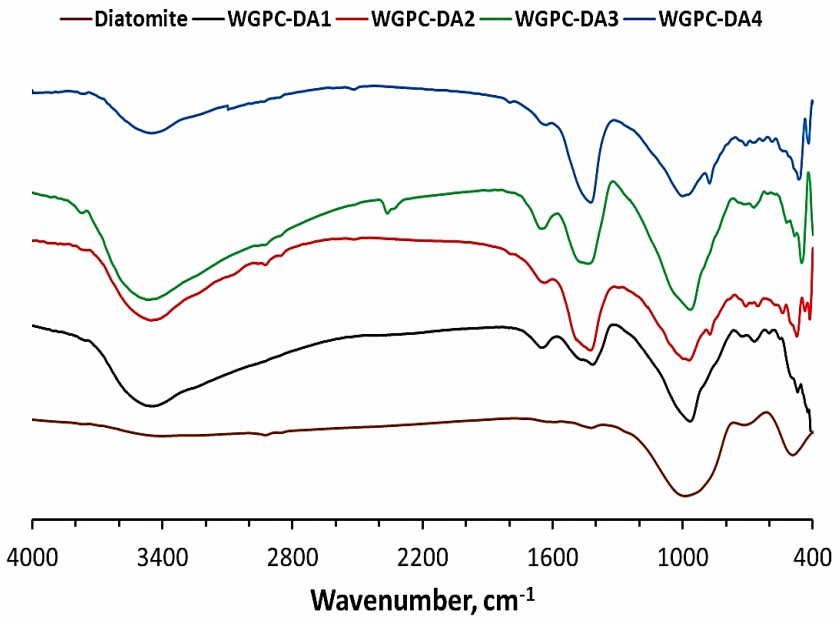

Fig. 15: FTIR-spectra of diatomite and the hardened one-part white geopolymer cements.

4.4.2. The potential application of eco-friendly magnesia-silicate cement in CO_2 sequestration.

Interestingly, reactive magnesium oxide-volcanic ash blends can react with water to yield hardened materials with acceptable mechanical properties. The exposure of the hardened materials to accelerated carbonation causes a significant change their performances.

4.4.2.1 XRD-analysis

The X-ray diffractograms **Fig. 16,** proved that brucite {$Mg(OH)_2$}, and periclase (MgO), quartz, and albite are the main phases of the hardened M-WVA mixture at zero time. The exposure of hardened material to CO_2 has resulted in the formation of nesquehonite ($MgCO_3$. $3H_2O$: PDF # 20-669). Same observation was reported by the previous work (**Liska et al., 2008; Vandeperre and Al-Tabbaa, 2007; Dung and Unluer, 2017)** as the nesquehonite phases has been formed in MgO-fly ash-Portland cement (PC) system. In contrast, **Abdel-Gawwad et al., (2019)** have reported that magnesium carbonate was formed during accelerated carbonation of hardened PC-MgO blends. The increase of exposure time leads to the enhancement of nesquehonite formation accompanied by the increase of $Mg(OH)_2$ consumption. $Mg(OH)_2$ acts as an active site for CO_2 capture as it can interact with hydrated CO_2 to yield nesquehonite mineral. It's worth mentioning that magnesium silicate hydrate (MSH: as the main binder of this system) is characterized by low crystallinity; so, it cannot be detected by XRD. This is in consistence with previous works **(Abdel-Gawwad et al., 2018b)**. As represented in **Fig. 17,** there is no difference between the mineralogical compositions of the hydration and carbonation products of M-WVA and M-RVA samples. Nevertheless, the pattern affiliated to M-RVA sample exhibits brucite mineral with lower peak intensity compared to that identified in the case of M-WVA one. This gives strong evidence on the high efficacy of M-RVA in the sequestration of CO_2.

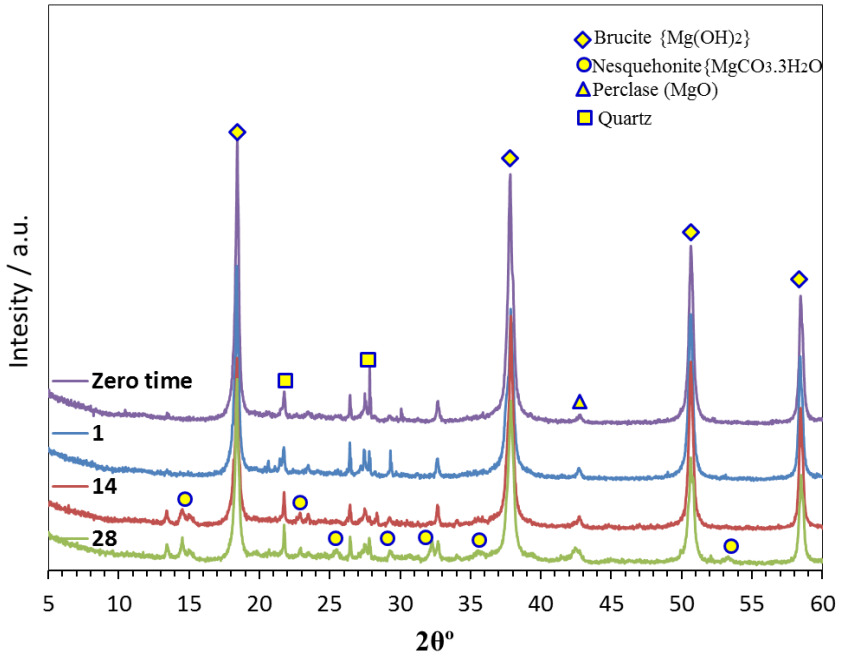

Fig. 16. XRD-patterns of the hardened carbonated M-WVA mixtures at different times of CO_2-exposure

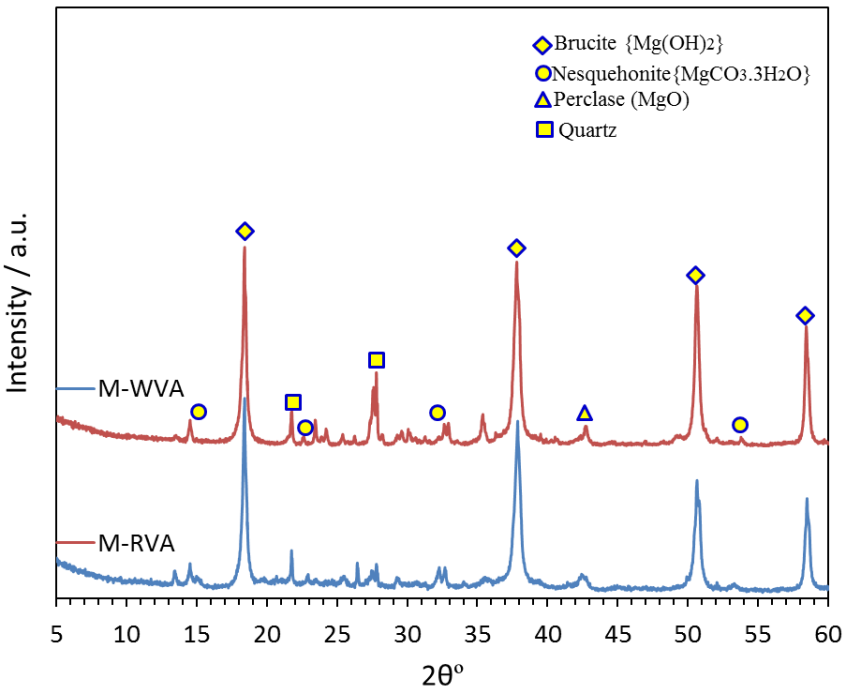

Fig. 17. XRD-patterns of the carbonated M-WVA and M-RVA mixtures at 28-days of CO_2-exposure

4.4.2.2. FTIR-spectroscopy

The FTIR spectra also confirmed that the transmittance bands affiliated to stretching vibration of CO_3^{2-} (at 1479 cm^{-1}) in the case of carbonated M-WVA was appeared with higher intensity compared to that identified in the case of zero time-hardened samples **Fig. 18.** The intensity of band characteristics for stretching vibration of OH within $Mg(OH)_2$ (at 3694cm^{-1}) decreases with CO_2 exposure time up to 28-days accompanied by an enhancement in CO_3^{2-} band intensity. This perfectly proves that the consumption of $Mg(OH)_2$ and the formation of carbonate containing phase are ongoing with time. It is important to note that, the intensity of transmittance bands related to bending vibration of HOH within MSH decreases with exposure time in the case of spectrum affiliated to hardened samples exposed to CO_2 gas for 28-days. This highlights the fact that the probability of MSH carbonation enhances with the increase of exposure time.

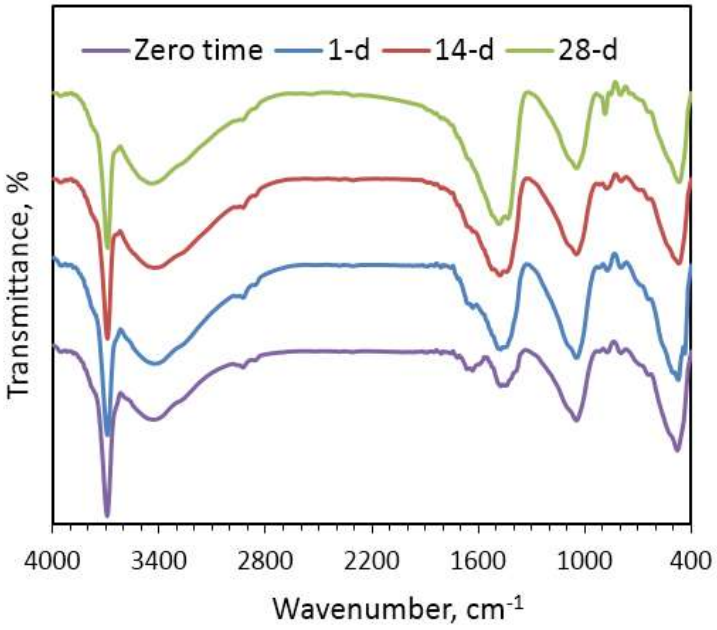

Fig. 18. FTIR-spectra of the carbonated M-WVA mixtures at different times of CO_2-exposure.

The intensity of a symmetric stretching vibration band of Si-O-Si(Al) (at 1043cm^{-1}) in the case of M-WVA seems to be with higher intensity comparing with that appeared in the spectrum of M-RVA **Fig. 19**. This proves the higher reactivity of WVA in the interaction with $Mg(OH)_2$, resulting in an enhancement in MSH formation. Complementary, the M-RVA spectrum exhibits OH band with $Mg(OH)_2$ with lower intensity compared with that

identified in the case of M-WVA one. This is an indication of the high efficiency of M-RVA sample in the capture of CO_2.

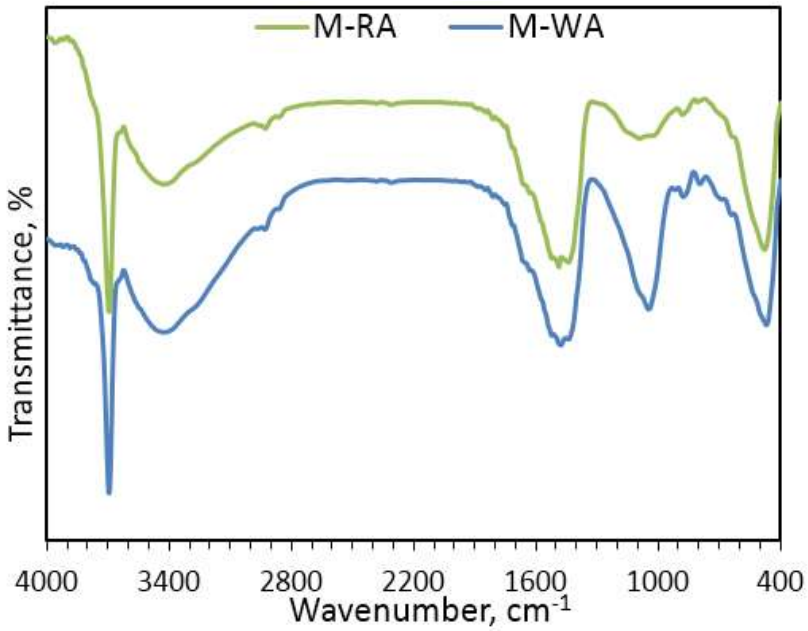

Fig. 19. FTIR-spectra of the carbonated M-WVA and M-RVA mixtures at 28-days of CO_2-exposure.

4.4.2.3. DTG-analysis

Fig. 20 represents the DTG-thermograms of M-WVA and M-RVA hydrated for 28-days (zero time). Different weight losses can be observed at different temperatures. The weight loss affiliated to the dehydration of combined water within MSH are detected at temperature range of 50-200 ºC **(Abdel-Gawwad et al., 2018a, b)**. The weight loss related to the dehydroxylation of $Mg(OH)_2$ was identified at 300-400 ºC **(Abdel-Gawwad et al., 2019)**. A small peak which appeared at 600-700 ºC is mainly referred to the decomposition of carbonate group within $MgCO_3$ **(Abdel-Gawwad et al., 2018a&b)**. The M-WVA demonstrates combined water weight loss within MSH greater than that of determined in the case of M-RVA at the same curing time. The sample with the higher MSH-weight loss (M-WVA) possesses the lower $Mg(OH)_2$ content and vice versa, confirming the strong relation between MSH formation and $Mg(OH)_2$ consumption during hydration process (before carbonation). This synergistic effect mainly depends on the amorphous content in volcanic ash. The reactivity of volcanic ash in the consumption of $Mg(OH)_2$ enhances with the increase of amorphous content in its microstructure. This is in line with previous work

(Abdel-Gawwad et al., 2018a), which reported that the silicate-rich-waste with high amorphous content has high efficacy on the consumption of $Mg(OH)_2$ and the formation of MSH.

The exposure of M-WVA to accelerated carbonation **Fig. 21** has resulted in the formation of new peak related to the dehydration of combined water (at 200-300ºC) within nesquehonite mineral ($MgCO_3.3H_2O$) accompanied by the increase of weight loss related to decarbonation of $MgCO_3$. With increasing exposure time, the weight loss of these phases increases associating with a noticeable decrease in $Mg(OH)_2$ weight loss. This should be explained by the capture of CO_2 by $Mg(OH)_2$ in the formation of carbonate-containing-phases. The M-WVA mixtures exposed for 28-days was found to exhibit the lowest MSH weight losses and the formation of the highest nesquehonite content. This is an indication of the potential impact of CO_2 on the carbonation of MSH resulting in the formation of carbonate-containing-phases. Comparing of the carbonated M-WVA, the exposure of M-RVA to CO_2 leads to the formation of higher nesquehonite weight loss **Fig. 22.** This could be related to the high availability of $Mg(OH)_2$, in the hydrated M-RVA at zero time **(See Fig. 20)** which acts as an active site for the capture of CO_2.

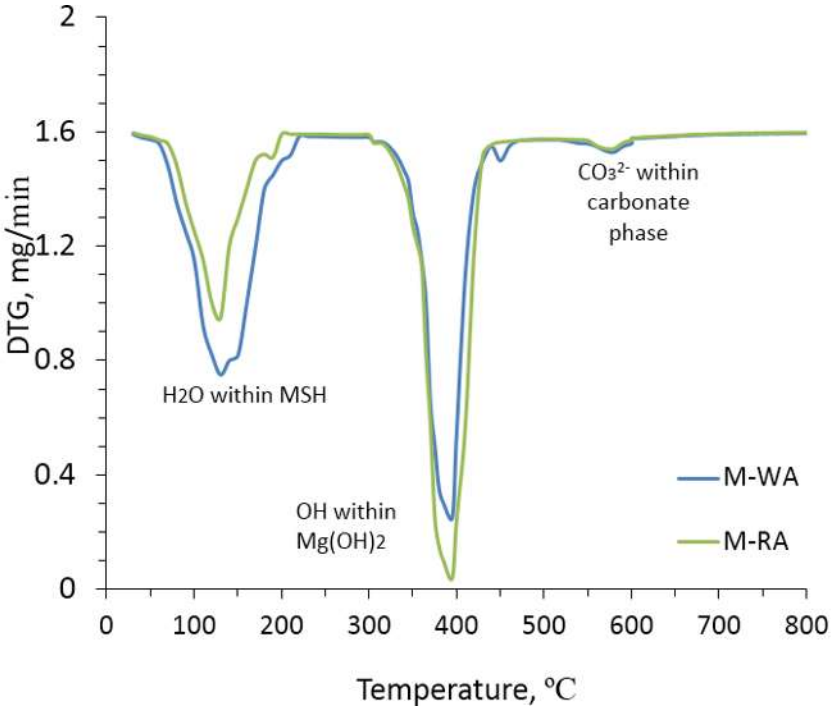

Fig. 20. DTG-thermograms of the hardened M-WVA and M-RVA mixtures at 28-days of curing in humidity

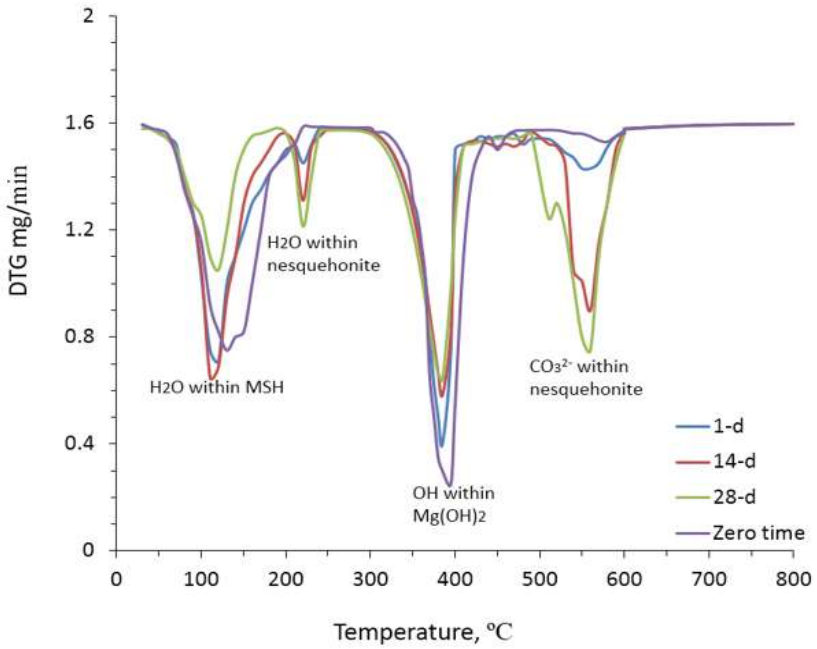

Fig. 21. DTG-thermograms the carbonated M-WVA mixture at different times of CO_2-exposure.

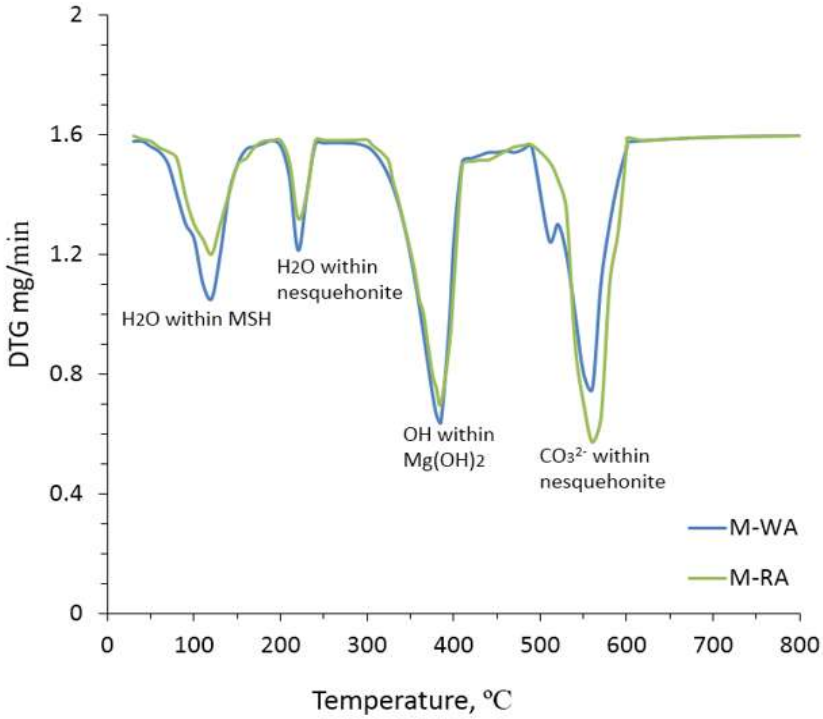

Fig. 22. DTG-thermograms of the hardened M-WVA and M-RVA mixtures at 28-days of CO_2-exposure.

Generally, the increase of weight loss (estimated by TGA) of hydrated and carbonated phases is an indication of the increment of their content. As reported in **Table 9**, the M-WVA mixture demonstrate MSH weight loss at zero time 35% higher than that recorded in the case of M-RVA one, indicating the significant role of amorphous content within volcanic ash in the uptake of hydrated magnesia and the formation of MSH-binder **(Abdel-Gawwad et al., 2018a)**. Both hydrated mixtures at zero time exhibit low carbonate loss, confirming the fact that the hydration is the dominant reaction which occurs during the curing of the hardened sample in 99±1 % RH, complying with previous work **(Abdel-Gawwad et al., 2018b)**. A considerable increase in $MgCO_3$ weight loss in parallel with a remarkable decrease in $Mg(OH)_2$ weight loss was detected with the increase of exposure time of the hydrated samples to CO_2. This demonstrates the carbonation process of the hydrated magnesia is ongoing with time. The weight loss of MSH slightly changes during the first 14-days of carbonation process, followed by a significant decrease in its value after 28-days of CO_2-exposure time. This means that after the first 14-days of accelerated carbonation, the MSH (responsible for the strength of hydrated samples) is carbonated by CO_2, yielding $MgCO_3$ (with lower binding capacity compared to MSH) and SiO_2 **(Eikeland et al., 2015; Wang et al., 2019)**. This explains why the compressive strength of the carbonated samples shift toward lower value at 28-days of curing **(See later Fig. 23).** At all carbonation ages, The M-RVA demonstrates CO_3 weight losses higher than those recorded in the case of M-WVA. This should be explained by the high availability of $Mg(OH)_2$ within the hydrated M-RVA (caused by the low pozzolanic activity of RVA) which represents active sites for carbonation reaction. The mathematical calculations prove that the intrusion of CO_2 sequestration by the hardened materials enhances with time. At 28-days of exposure time, the M-WVA and M-RVA samples absorb ~ 22 and 26% CO_2, respectively. This means that each ton of the prepared materials absorb ~220 and 260 kg/ton, respectively. This strongly contributes to the mitigation of the global warming potential (GWP) resulted from different industrial activities.

Table 9: TG-weight losses and calculated CO_2 content sequestrated by the prepared materials at different CO_2-exposure times.

Mixtures notations	Exposure time (day)	Weight loss wt. %				CO_2 wt. % ratio in the sample
		MSH	$Mg(OH)_2$	$MgCO_3$	Total loss	
M-WVA	0	3.20	4.12	0.38	10.49	3.62
	1	3.31	3.54	1.65	13.38	12.33
	14	3.39	2.16	2.89	14.75	18.09
	28	2.54	1.75	3.54	15.97	22.16
M-RVA	0	2.36	5.16	0.45	11.25	4.01
	1	2.41	3.28	2.19	13.51	16.21
	14	2.45	2.14	3.26	14.99	21.74
	28	2.01	1.86	4.19	16.04	26.12

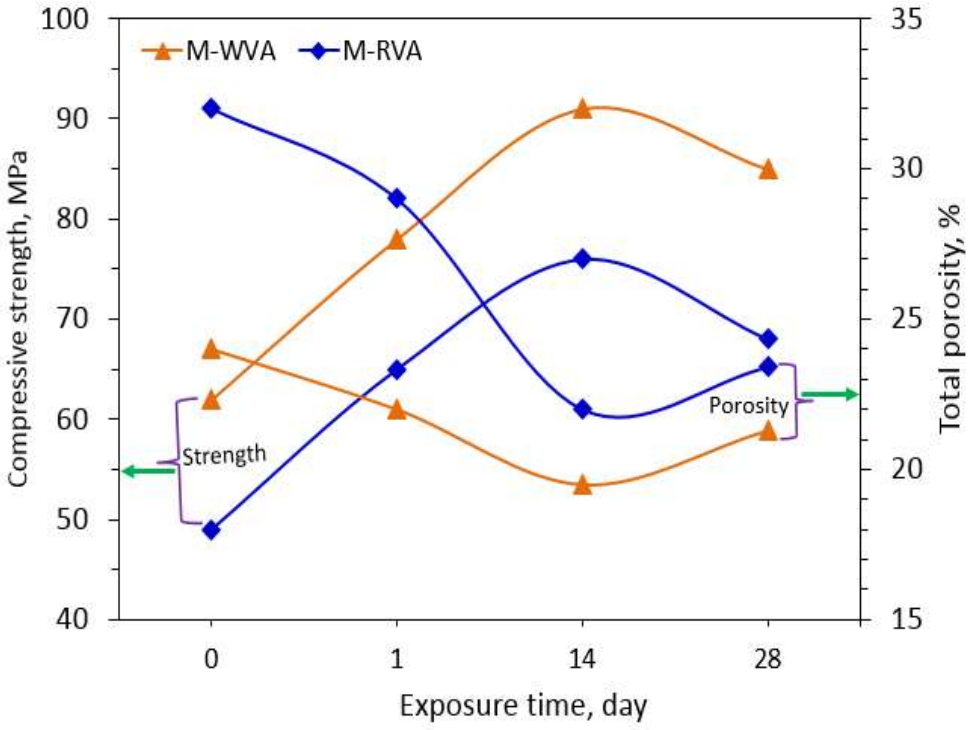

Fig. 23. Relationship between strength and porosity of the carbonated samples exposed to CO_2-gas at different times.

4.4.2.4. Physical and mechanical properties

The relationship between compressive strength development and porosity of the carbonated samples at different ages is displayed in **Fig. 23.** Firstly, the hardened M-WVA and M-RVA at zero time demonstrate compressive strength values of 62 and 49MPa, respectively. This variation in strength is mainly due to the change in amorphous content in each volcanic ash, meaning that the physical nature of volcanic ash plays a circular role in the performance of the hardened material **(Abdel-Gawwad et al., 2018a)**. As proved by Rietveld XRD-quantitative analysis, WVA represents amorphous content (72 %) higher than that recorded by RVA (39 %). The ash with high amorphous content exhibits high capability to interact with $Mg(OH)_2$, yielding excessive content of MSH binding phase, complying with TG/DTG and FTIR-analyses. At the first 14-days of carbonation, a significant increase in compressive strength associating with porosity reduction has been recorded. The positive role of accelerated carbonation on strength development and porosity reduction has been observed in the case of different cementitious systems having MgO **(Morrison et al., 2016).** The reason behind this effect is the increase of CO_2-capture **(See Fig. 24),** yielding carbonate-containing-phases.

The accumulation of carbonate phases mainly contributes to the reduction of pore volume of the hardened material. Moreover, the CO_2-capture has no effect on MSH-binder formed in the hardened matrix at this period (Fig. 11). Interestingly, the hardened M-WVA mixture exposed to CO_2 for 14-days represents compressive strength value higher than that of the hydrated sample (at zero time) by ~47 % accompanied by the lower porosity. Although the hardened M-RVA mixture shows compressive strength values lower than those of M-WVA one, it records compressive strength development higher than that of M-WVA mixture, especially at 14-days of CO_2-exposure (55 %). This should be explained by the higher zero-time porosity (32 %) of the hardened M-RVA compared to that of M-WVA one (24%). The higher porosity has potential impact on the acceleration of carbonation rate including the fast intrusion of CO_2-gas into the hardened materials (**Morrison et al., 2016).** The high porosity of the hardened M-RVA mixture at zero time is due to the low amorphous content in RVA as it has low efficacy in the interaction with hydrated magnesium oxide, resulting in the formation of low MSH-content. Moreover, the high crystallinity of RVA causes the

formation of excessive $Mg(OH)_2$ content which in turn easily transforms to nesquehonite after exposure of hardened material to CO_2.

It is postulated that the rate of CO_2 diffusion into the hardened material enhances with the increase of its pore volume, confirming the higher CO_2-capture in the case of M-RVA sample as compared with M-WVA one. The 28-days carbonated samples demonstrate the highest CO_2-capture **Fig. 24.** Nevertheless, they represent compressive strength lower than those of 14-days carbonated ones **Fig. 23.** This is likely derived from the fact that the continuous exposure of hardened samples to CO_2 has resulted in a significant reduction in MSH-content within hardened matrix, complying with TG/DTG results. It can be said that regardless the role of amorphous content in volcanic ashes in prepared materials, it potentially affects the rate of CO_2 capture within hardened materials.

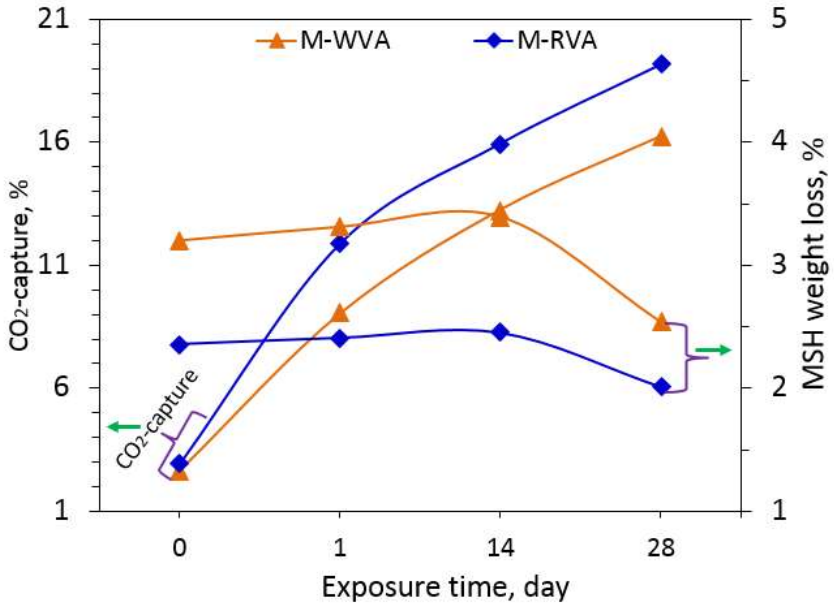

Fig. 24. Relationship between CO_2-capture and MSH content of the carbonated samples exposed to CO_2-gas at different times.

4.4.2.5. Mechanism of accelerated carbonation

The reaction mechanism of CO_2-sequestration by the fabricated materials is shown **in Fig. 25 (Fernández Bertos et al., 2004)**. The capture process initiates by the diffusion and penetration of CO_2-gas through the hardened materials, followed by transformation of CO_2 from gas state to liquid one (H_2CO_3: as intermediate step). This transformation is caused by

the high moisture content within hardened materials. Carbonic acid (H_2CO_3) is unstable compound which immediately ionized to H^+, HCO_3^-, and CO_3^{2-}. Carbonate ions interact with $Mg(OH)_2$ (as a byproduct of the hydration of MgO-volcanic ashes mixtures), yielding nesquehonite ($MgCO_3.3H_2O$). At later ages, MSH (as the main binder of the hardened materials) can be carbonated to form silicate hydrate and $MgCO_3.3H_2O$, resulting in a significant loss in mechanical properties. As shown in **Fig. 26,** a noticeable change in the color of hardened materials was recorded when they exposed to accelerated carbonation, confirming the formation of carbonate phase caused by CO_2-caprture by these materials.

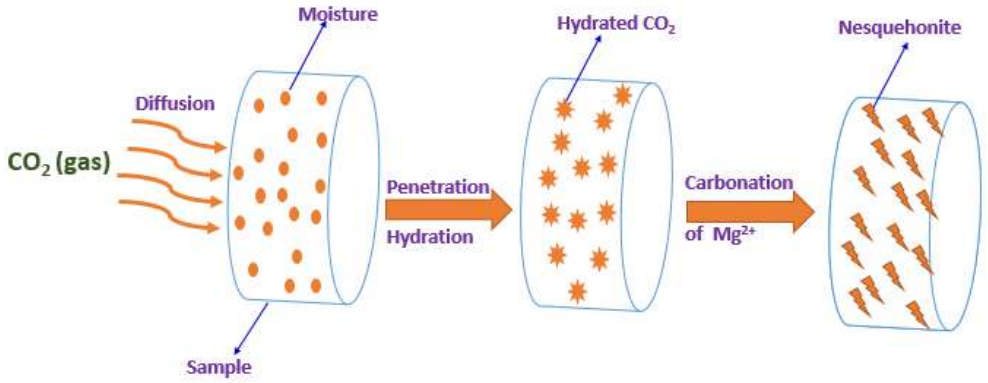

Fig. 25. Proposed reaction mechanism of the accelerated carbonation adapted from **(Fernández Bertos et al., 2004)**.

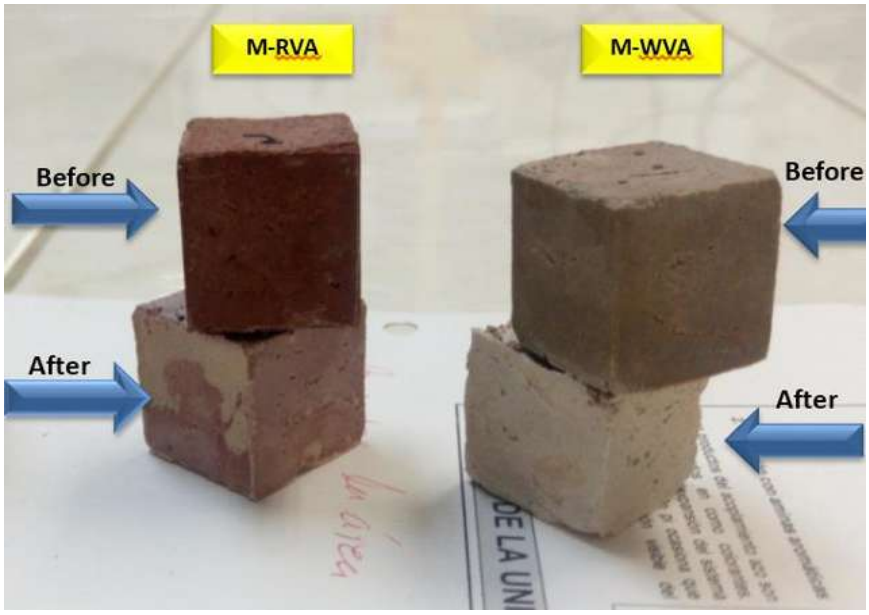

Fig. 26. Digital photos of hardened samples before and after accelerated carbonation.

4.4.2.6. Beneficial use of the prepared materials

The above-mentioned outcomes proved that the designed hardened materials from naturally occurring volcanic ashes and MgO were found to have high efficacy in the CO_2-capture accompanied a remarkable change in their physical and mechanical properties. Moreover, the proposed method in the present study can be beneficially applied in the sustainable disposal aluminosilicate and magnesia-rich-wastes in the cleaner production of cementitious materials with high performance and efficacy in the sequestration of CO_2-gas. This not only strongly contributes to the conservation of naturally occurring resources used in construction, but also reflects on the mitigation of global warming potential caused by industrial and human activities.

4.4.3. The creation of a geopolymer foam with high thermal insulation properties from Coconut ashes wastes

This is the last specific objectives and it is results and discussion will be in the following points:

4.4.3.1. Optimization of alkali concentration

In order to optimize the concentration of alkali activator required to produce geopolymer with high mechanical properties, coconut ashs (CA) was activated by 4, 5 and 6 wt.,% NaOH. The compressive strength values of CA-based geopolymer activated by different NaOH concentrations are shown in **Fig. 27.** Evidently, the compressive strength of all mixes increases with curing time up to 28 days. This highlights the continuation of CA activation and formation of geopolymeric binder with time. the increase of NaOH concentration up to 5% leads to enhance the compressive strength of CA. Meanwhile, a further increase in akali concentration (6 wt. %) has a negative impact on strength. The CA-5 found to be the optimum mix, giving 28-days compressive strength of 73 MPa, meaning the 5 wt., % is the desirable NaOH mass%. The low NaOH leads to decrease dissolution rate and produce little activated species extent. Although the high alkali concentration accelerates the dissolution of aluminosilicate rate, it causes the hinderance of condensation process **(Abdel Gawwad et al., 2016)**. The optimum CA-based geopolymer (CA-5) showed a bulk density of 1.45 g/cm3 and total porosity of 23% at 28-days of curing.

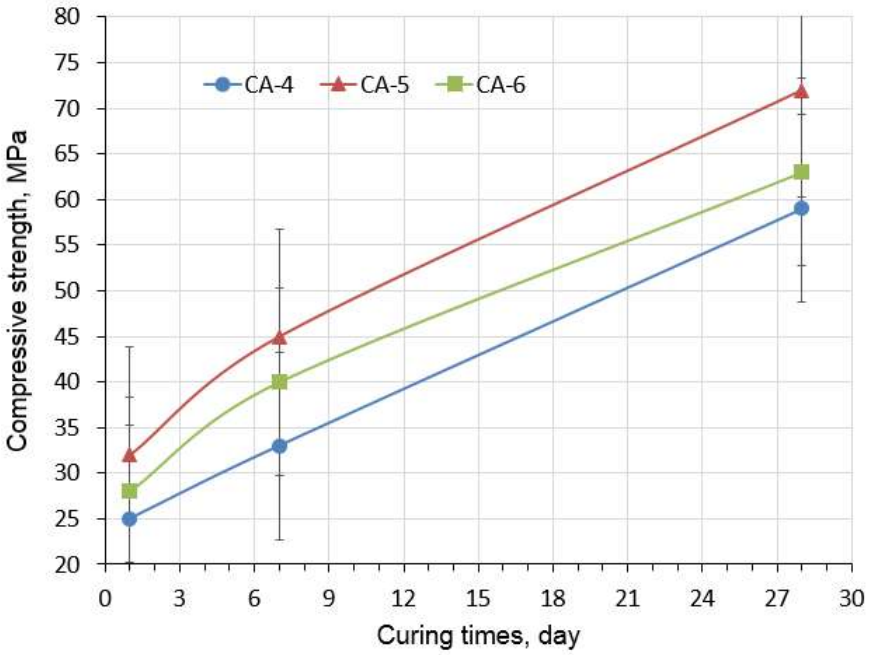

Fig. 27: Compressive strength of alkali activated unfoamed CA-based geopolymer.

4.4.3.2. CA-based geopolymer foam

Porosity including pore size and structure, bulk density, mechanical properties, and thermal conductivity are the main parameters which affect the performance of porous or foamed geopolymer **(Abdollahnejada et al., 2015; Baia et al., 2016; Bell and Kriven, 2009 ; Novais et al., 2016).** An experimintal study was carried out in order to investigate the effect of alumina slag (AS) content (as innovative foaming agent), and water content on the properties of geopoymer foam (GPF).

As shown in **Fig. 28**, the AS content potentially affects the compressive strength of CA-based geopolymer. The compressive strength decreases by 42, 69, and 96% with the addition of 3, 5 and 7 wt% AS, respectively. In parellel, the bulk density of activated CA varied from 1.45 to 0.75 g/cm3 with the increase of AS content. Fig. 3 also proved that the total porosity significanly increases with AS addition to reach 78% in case of GPF containing 7 mass% AS.

Fig. 29 proved that there is a proportional releationship between total porosity and thermal conductivity. When the total porosity increases (with the increase of AS content), the thermal conductivity of GPF remarkably decreases. It is distinguished that, the GPF with

high AS content exhibits the lower compressive strength, bulk density and thermal conductivity as well as higher total porosity as compared with the unfoamed GP-sample.

As a second parameter, the water to coconut as powder (W/CA) strongly effects on the performance of GPF. **Fig. 30** represents the compressive strength, bulk density and total porosity values of GPF containing 7 mass% AS as a function of W/CA ratios. A significant compressive strength, bulk density reduction as well as total porosity increment have been observed with the increase of W/CA ratio up to 0.4. In contrast, the thermal conductivity of GPFs being reduced with the increase of mixing water **Fig. 31.** The GPF containing 7 mass% AS with W/CA ratio of 0.40 possess the lowest compressive strength (1.3MPa), bulk density (0.64 g/cm3) and thermal conductivity (0.045 W/mk), and the highest total porosity (83%).

The possible explanation of the these findings is with the increase of AS and content and W/CP ratio, the rate of H2 gas liberation enhances, causing the increase of pores content and sizes which in turn leads to create GPFs with higher porosity as well as lower compressive strength, bulk density and thermal conductivity.

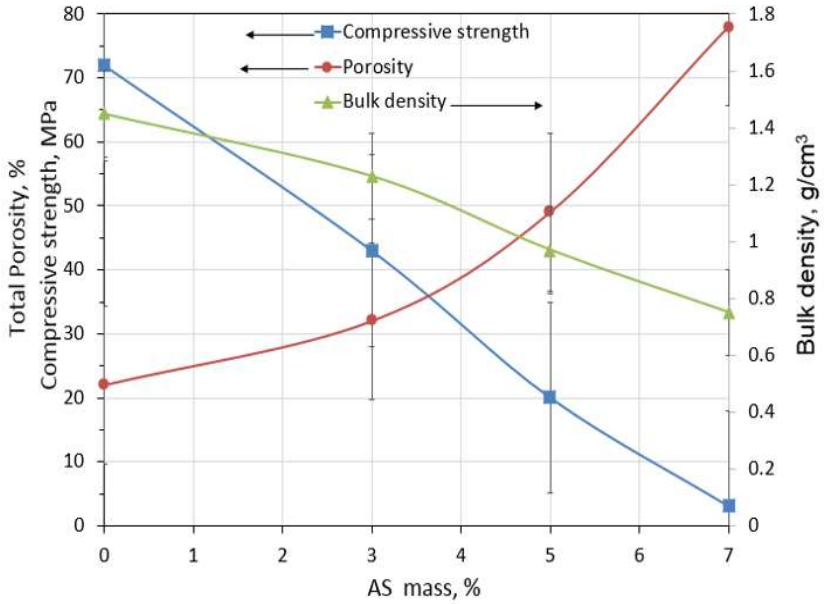

Fig. 28: Relationship between total porosity, compressive strength and bulk density of CA-geopolymer foam as a function of AS content.

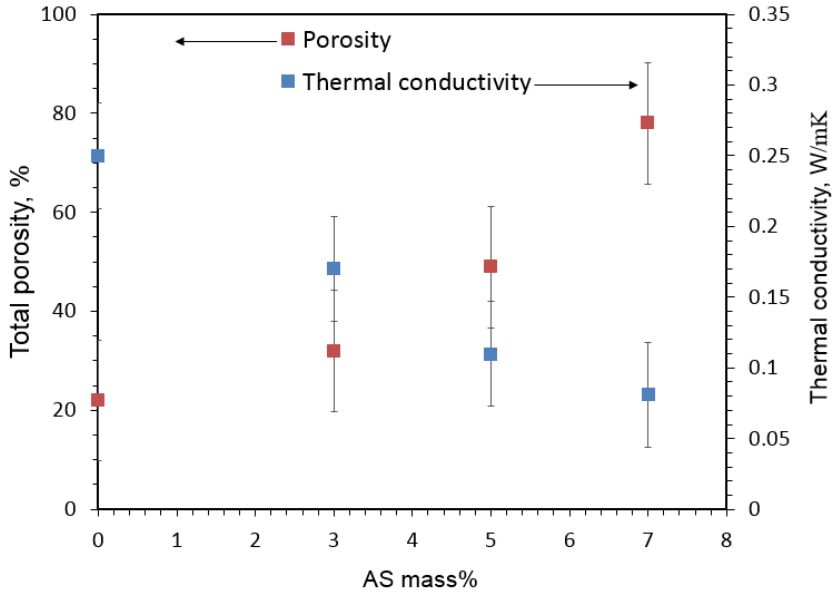

Fig.29: Relationship between total porosity and thermal conductivity of CA-geopolymer foam as a function of AS content.

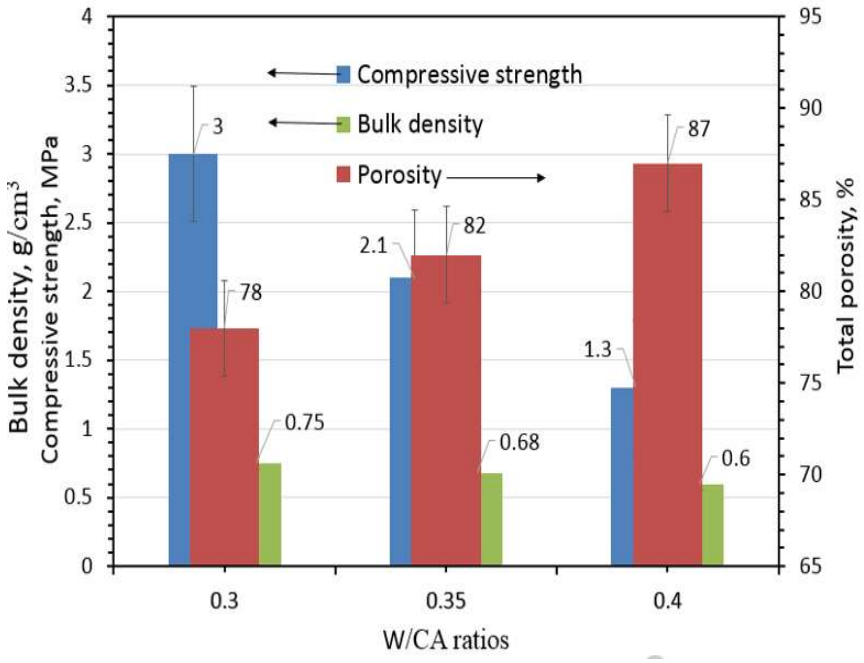

Fig.30: Compressive strength, bulk density and total porosity of CA-geopolymer foam as a function of W/CA ratio.

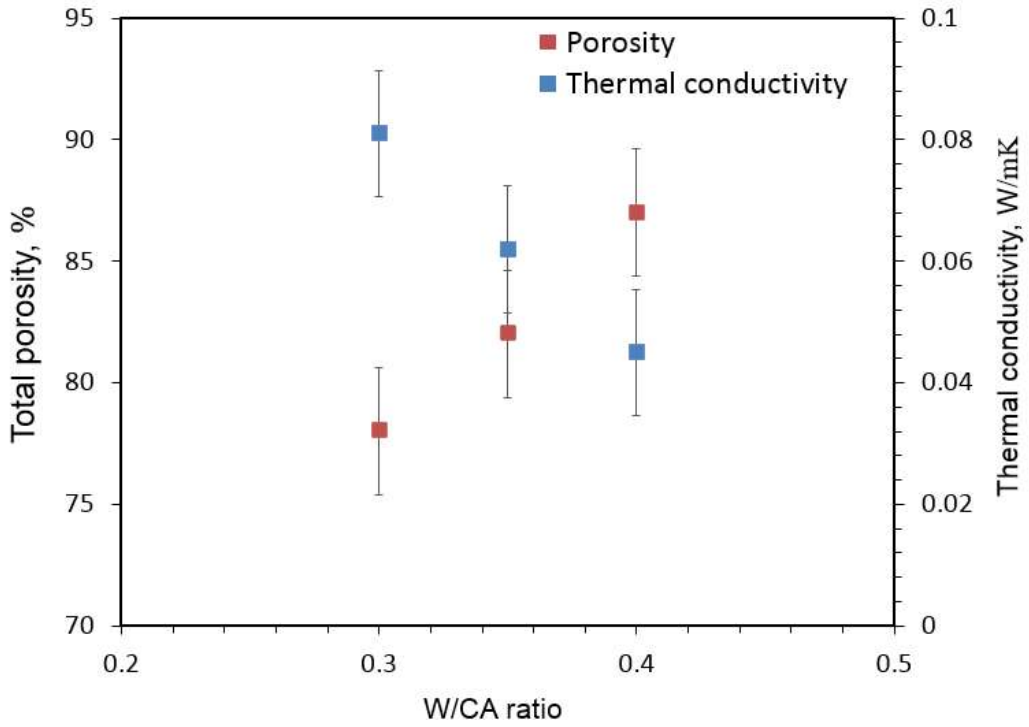

Fig.31: Relationship between total porosity and thermal conductivity of CA-geopolymer foam as a function of W/CA ratio.

The SEM-photographs and digital photos of CA-based geopolymer foams are displayed in **Fig. 32.** It's clear that, in **Fig. 32 (A & B)** SEM at two magnifications scale as well as **(Fig.32 C)** digital photos of CA-5/AS3, CA-5/AS5, CA-5/AS7, and CA-5/AS7-2 (from top to bottom). The SEM-photographs and digital photos showed that that the pores content and sizes increase with the increase of AS content and W/CA ratio. Pores with average size of ~55 µm was obsereved in case of CA-5/AS3 microstructure. The addition of 5wt.% AS (CA-5/AS5) leads to increase the average pore size to reach ~120 µm. The microstructure of CA-5/AS7 has the largest pore size of ~185 µm. The microstructure of CA-5/AS7-2 represented the greatest average pore size of ~210 µm, confirming the positive impact of water in the enhancement of pores formation. The results of compressive strength, bulk density, porosity, thermal conductivity, and SEM-photographs are in a good harmony to each other.

The whole technique used to recycle the coconut ashes (CA) to fabricate thermally insulating materials using alkali activation of coconut ashes (CA), in the presence of alumina slag as innovative foaming agent, can be concluded in the **Fig. 33.**

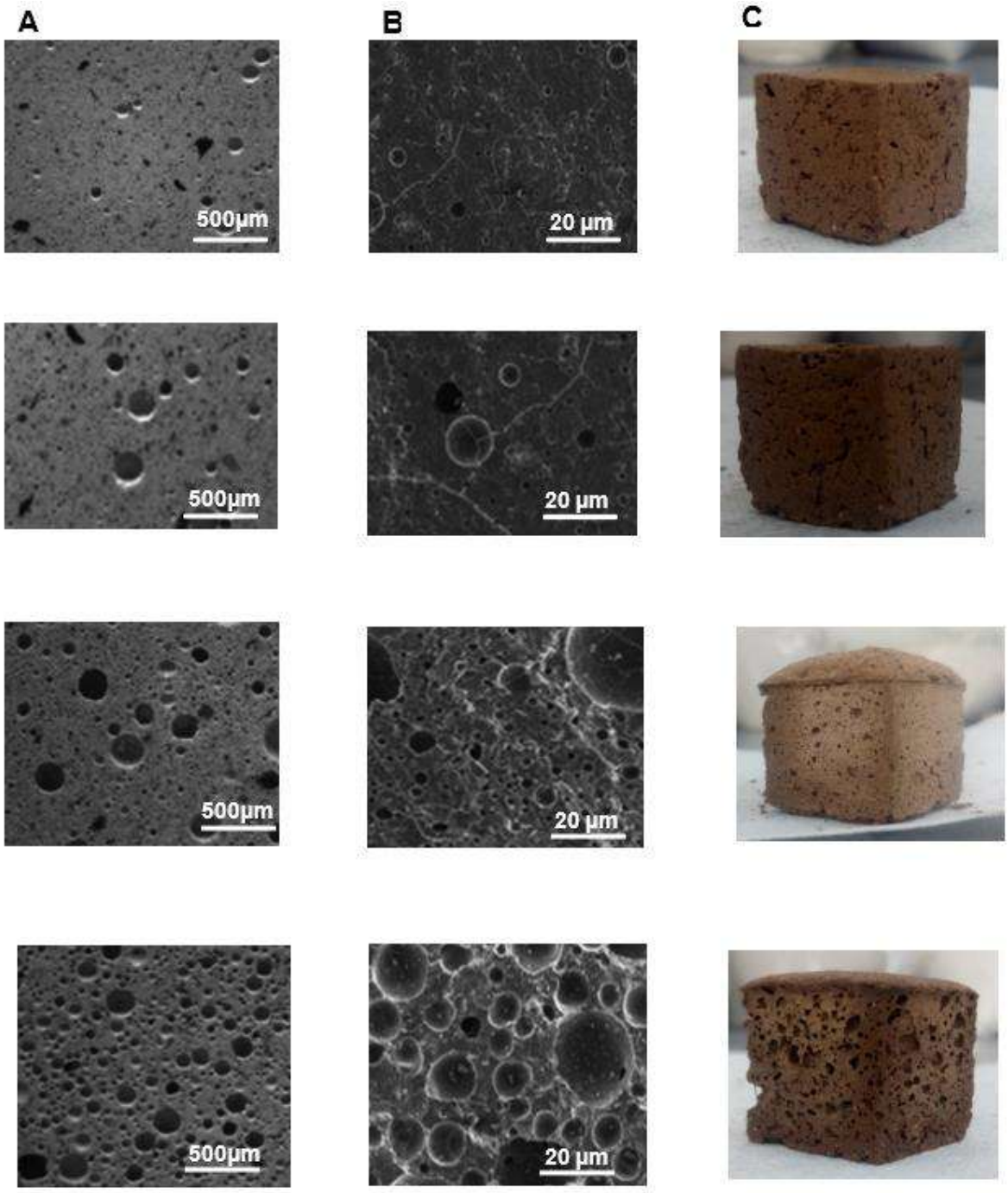

Fig.32: (A & B) SEM at two magnifications scale as well as (C) digital photos of CA-5/AS3, CA-5/AS5, CA-5/AS7, and CA-5/AS7-2 (from top to bottom).

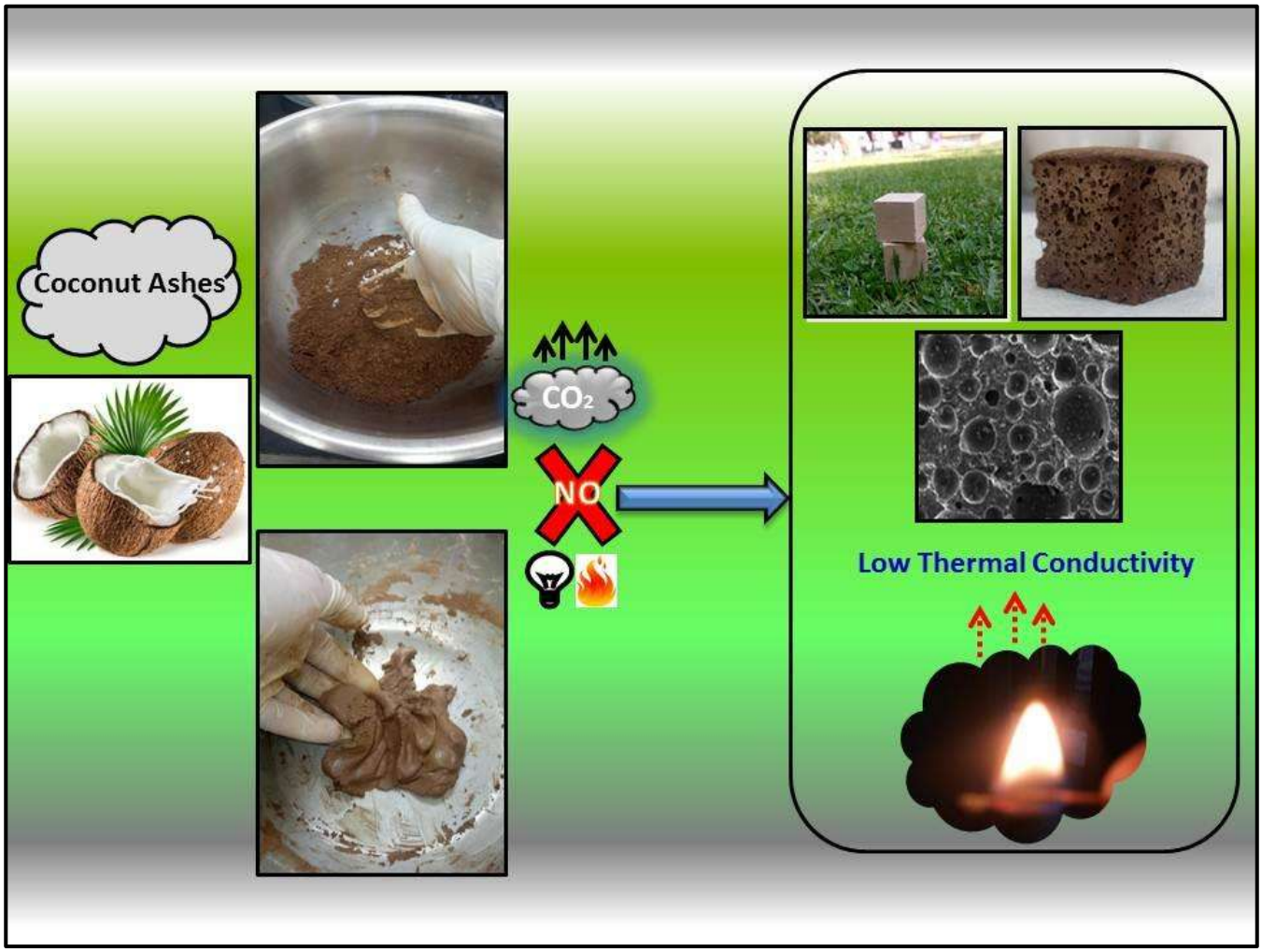

Fig.33: Describe the whole technique used to recycle coconut ashes to fabricate a porous coconut ash (CA)-based geopolymer foam with high thermal insulation property.

CHAPTER V
CONCLUSION

The work here focused on achieving the specific objectives by utilizing different techniques with different raw materials. Concerning to the first specific objective which is creating a cement material with good mechanical properties from utilizing of both Wood biomass ashes and diatomite. A valorization of wood biomass ash in designing one-part white geopolymer cement using diatomite as main precursor was investigated. Dry activator was prepared by treated $CaCO_3$-rich wood biomass ash with NaOH at different $NaOH/CaCO_3$ molar ratios. White color and high calcium content are the main advantages of the prepared dry activator to be suitable for blending with naturally accruing diatomite (with white color), to produce one-part white geopolymer cement which hardened at 23±2ºC after mixing with water like Portland cement. The content of pre-treated wood biomass ash added to diatomite increases with the decrease of $NaOH/CaCO_3$ molar ratio to achieve 3 wt. % NaOH equivalent in all mixes. Different performances of the prepared cement have been detected depending on the content of pre-treated wood biomass ash. The low (8 wt. %) and high (43 wt. %) pre-treated wood bio content demonstrated the 28-days strengths of 36 and 27MPa, respectively. The optimum pre-treated wood bio content of 21.5 wt. % demonstrated compressive strength of 48MPa at the same curing time. The second specific objective which is creation of magnesium silicate cement with good mechanical properties and the ability to absorb the CO_2 from the air in both long and short terms. The work focused on the impact of accelerated carbonation on the performance of the hardened magnesium silicate cement under humidity and accelerated carbonation conditions. These materials were fabricated by mixing magnesium oxide-volcanic ashes blends with water, followed by humidity curing. As proved by different analyses, magnesium silicate hydrate and magnesium hydroxide are the main hydration products within fabricated materials. Magnesium hydroxide was found to be the active site for CO_2-capture, resulting in the formation of nesquehonite phase in the open pores of the hardened mixtures. The amorphous content in volcanic ashes plays a circular role in the performance of the fabricated materials and their ability to CO_2-capture. The fabricated material containing volcanic ash with low amorphous content represented the higher effectiveness in the CO_2-sequestration compared to that having high amorphous content. The main reasons behind

this criterion are the formation of porous hardened material and the enhancement of magnesium hydroxide availability. The beneficial use of these materials in different engineering projects is not only based on their high efficacy in the CO_2-capture, but also due to the enhancement of their physical and mechanical properties with CO_2-exposure.

Finally, the achieving of the last objective which is fabrication of a thermal insulator cement material from coconut ash wastes. This work deal with the preparation of geopolymer foam using a new aluminosilicate agriculture wastes (coconut ashes) and alumina slag as foaming agent. Geopolymer foam was synthesized by recycling of coconut ashes wastes and mixed with alumina slag powder in presence of sodium hydroxide solution. The results proved that the increase of alumina slag and mixing water led to produce geopolymer foam with low thermal conductivity, bulk density, and compressive strength as well as high porosity. SEM-photographs confirmed that the pore size of geopolymer foam mainly depended on the alumina slag content and water to coconut powder ratio. The prepared geopolymer foam can be beneficially used as light weight thermally insulating materials for many applications. Also, the low thermal conductivity CA-based geopolymer foam is a novel eco-friendly product due to fabrication at room temperature (no firing process). Meanwhile, the utilization of coconut ashes (CA), decreases environment pollution and creates clean green environments.

CHAPTER VI
REFERENCES

Abdel Gawwad, **H. A., Khater, H. M., Abd El-Aleem, S., 2016.** Coupled effect of alkali concentration and metakaolin content on accelerated ageing of slag. Geosystem Engineering 19, 125-132.

Abdel-Gawwad, H. A, Abo El-Enein, S.A., 2016. A novel method to produce blended geopolymer cement powder. HBRC. J. 12(1), 13-24.

Abdel-Gawwad, H. A., Khalil, Kh. A., 2018. Application of thermal treatment on cement kiln dust and feldspar to create one-part geopolymer cement. Constr. Build. Mater. 187, 231-237.

Abdel-Gawwad, H. A., Abd El-Aleem, S., 2015. Effect of reactive magnesium oxide on properties of alkali activated slag geopolymer cement pastes. Ceramics – Silikay 59 (1), 37-47.

Abdel-Gawwad, H. A., Abd El-Aleem, S., Ouda, A.S., 2016. Preparation and characterization of one-part non-Portland cement. Ceramics International 42, 220–228.

Abdel-Gawwad, H. A., García S.R.V., Hassan H. S., 2018a. Thermal activation of air-cooled slag to create one-part alkali activated cement. Ceramics International Journal 44(12), 14935-14939.

Abdel-Gawwad, H. A., Mohamed, S. A., Mohammed, M. S., 2019. Recycling of slag and lead-bearing sludge in the cleaner production of alkali activated cement with high performance and microbial resistivity. Journal of Cleaner Production 220, 568-580.

Abdel-Gawwad, H.A., Abd El-Aleem, S., Abo El-Enein, S.A., Khalifa, M., 2018b. Resistivity of ecofriendly alkali activated industrial solid wastes against sulfur oxidizing bacteria. Ecological Engineering 112, 1-9.

Abdel-Gawwad, H.A., Abo-El-Enein, S.A., 2016. A novel method to produce dry geopolymer cement powder, HBRC J. Vol. 12 ,13–24.

Abdollahnejada, Z., Pacheco-Torgala, F., FélixbW, T., Aguiar, J.B., 2015. Mix design, properties and cost analysis of fly ash-based geopolymer foam. Construction and Building Materials. 80, 18-30.

Adesanya, E., Ohenoja, K., Luukkonen, T., Kinnunen, P., 2018. One-part geopolymer cement from slag and pretreated paper sludge. Journal of Cleaner Production 185, 168-175.

Aiken, T.A., Sha, W., Kwasny, J., Soutsos, M.N., 2017. Resistance of geopolymer and Portland cement-based systems to silage effluent attack, Cem. Concr. Res. Vol. 92 ,56–65.

Andrew, R.M., 2017. Global CO_2 emissions from cement production, Earth Syst.Sci. Data. Discuss. In review https://doi.org/10.5194/essd-2017-77.

ASTM C109/C109M, 2016. Standard Test Method for compressive strength of hydraulic cement mortars.

ASTM C191, 2013. Standard Test Methods for Time of Setting of Hydraulic Cement by Vicat Needle.

Bagheri, A., Nazari,A., Hajimohammadi, A., Sanjayan, J. G., Rajeev, P., Nikzad, M., Ngo, T., Mendis, P., 2018. Microstructural study of environmentally friendly boroaluminosilicate geopolymers. J. Clean. Prod. 189, 805-812.

Baia, C., Franchina, G., Elsayeda, H., Contea, A., Colombo, P., 2016. High strength metakaolin-based geopolymer foams with variable macroporous structure. J. Europ. Cer. Soc. 36, 4243-4249.

Bakharev, T. , Sanjayan, J. G., Cheng, Y. B., 2003. Resistance of alkali-activated slag concrete to acid attack. Cem.Concr. Res. 33(10), 1607-1611.

Bakharev, T. 2005. Resistance of geopolymer materials to acid attack. Cem.Concr. Res. 35(4), 658-670.

Bakharev, T., 2005. Resistance of geopolymer materials to acid attack, Cem. Concr. Res. Vol. 35,658–670.

Bakri, A. M., Mustafa, A., Liyana, J., Kamarudin, H., Bnhussain, M., Ruzaidi, C. M., Rafiza, A. R., Izzat, A. M. 2013. Study on Refractory Materials Application Using Geopolymer Processing. Advanced Science Letters 19, 221-223.

Barnard, R., 2014. Mechanical properties of fly ash/slag based geopolymer concrete with the addition of macro fibres. Master thesis, Faculty of Engineering, Stellenbosch University, South Africa.

Bell, J.L., Kriven, W.M., 2009. Preparation of Ceramic Foams from Metakaolin-Based Geopolymer Gels. Ceramic Engineering and Science Proceedings 29, 96–111.

Brough, A.R., Holloway, M., Sykes, J., Atkinson, A., 2000. Sodium silicate-based alkali activated slag mortars. Part II. The retarding effect of additions of sodium chloride or malic acid, Cem. Concr. Res. Vol. 30,1375–1379.

Carabba, L., Manzi, S., Bignozzi, M.C., 2016. Superplasticizer addition to carbon fly ash geopolymers activated at room temperature, Mater. Vol. 9,586.

Catauro, M., Bollino, F., Lancellotti, I., Kamseu, E., Leonelli, C., 2010. Chemical and biological characterization of geopolymers for potential application as hard tissue prostheses. Advances in Science and Technology Vol. 69, 192-197.

Camiletti, J., Soliman A., Nehdi M., 2013. Effect of nano-calcium carbonate on early-age properties of ultrahigh- performance concrete. Magaz. Concr. Res. 65 (5), 297-307.

Chandrasekhar, S., Satyanarayana, K.G., Pramada, P.N., Raghavan, P., Gupta, T.N., 2003. Processing, properties and applications of reactive silica from rice husk - an overview, J. Mater. Sci. Vol. 38,3159–3168.

Chang, J.J., 2003. A study on the setting characteristics of sodium silicate-activated slag pastes, Cem. Concr. Res. Vol. 33,1005–1011.

Chindaprasirt, P., De Silva, P., Sagoe-Crentsil, K., Hanjitsuwan, S., 2012. Effect of SiO2 and Al2O3 on the setting and hardening of high calcium fly ash-based geopolymer systems, J. Mater. Sci. Vol. 47, 4876–4883.

Choo, H., Lim, S., Lee, W., Lee, C., 2016. Compressive strength of one-part alkali activated fly ash using red mud as alkali supplier, Constr. Build. Mater. Vol. 125, 21–28.

Damtoft, J.S., Lukasik, J., Herfort, D., Sorrentino, D., Gartner, E.M., 2008. Sustainable development and climate change initiatives, Cem. Concr. Res. Vol. 38,115–127.

Davidovits, J., 1988. Geopolymer chemistry and properties", In: Proceedings of 1988 geopolymer conference, 1, 25–48.

Davidovits, J., 1988. Geopolymer Chemistry and Properties. 1st International Conference on Geopolymer. Compiegne, France, 1-3 June 1988. Saint-Quentin: Geopolymer Institute.

Davidovits, J., 2013. Geopolymer Cement: A Review. Geopolymer Institute: Saint Quentin.

Davidovits, J., 2015. Geopolymer chemistry and applications. 4th edition, Institut Géopolymère Saint-Quentin, France.

Davidovits, J., 2015. Geopolymer Chemistry&Applications, 4th ed., Institut Geopolymere, Saint-Quentin, pp. 558–568.

Davidovits, J., 2015. Calcium based geopolymer,in :J.Davidovits(Ed.), Geopolymer Chemistry and Applications,3rd-ed.,Geopolymer Institute, Saint Quentin, France, pp.201–244.

Della, V.P., Kühn, I., Hotza, D., 2002. Rice husk ash as an alternate source for active silica production, Mater. Lett. Vol. 57, 818–821.

Ding, Y.-C., Cheng T.-W., Dai, Y.-S., 2017. Application of geopolymer paste for concrete repair. Structural Concrete 18(4), 561-570.

Djobo, J.N., Elimbi, A., Tchakouté, H.K., Kumar, S., 2016. Mechanical activation of volcanic ash for geopolymer synthesis: effect on reaction kinetics, gel characteristics, physical and mechanical properties, RSC Adv. Vol. 6 ,39106–39117.

Duxson, P. Provis, J.L., 2008. Designing precursors for geopolymer cements, J. Am. Ceram. Soc. Vol. 91, 3864–3869.

Duxson, P., and Provis, J.L., 2008. Designing precursors for Geopolymer Cements. Journal of the American Ceramic Society, 91(12) pp. 3864-3869.

Duxson, P., Fernandez-Jimenez, A., Provis, J.L., Lukey, G.C., Palomo, A. and van Deventer, J.S.J., 2007. Geopolymer technology: The current state of the art. Journal of Materials Science, 42(9) pp. 291 -2913.

Duxson, P., Geopolymer precursor design, in: **Provis, J.L., Van Deventer, J.S.J., 2009.** (Eds.), Geopolymers: Structures, Processing, Properties and Industrial Applications, Woodhead publishing Ltd and CRC Press, Cambridge and Boca Raton, pp. 37–49.

Eikeland, E., Blichfeld, A.B., Tyrsted, C., Jensen, A., Iversen, B.B., 2015. Optimized Carbonation of Magnesium Silicate Mineral for CO2 Storage. ACS Applied Materials & Interfaces 7 5258-5264.

Flatt, R.J., Roussel, N., Cheeseman, C.R., 2012. Concrete: an eco-material that needs to be improved, J. Eur. Ceram. Soc. Vol. 32,2787–2798.

Fernández Bertos, M., Simons, S.J., Hills, C.D., Carey, P.J., 2004. A review of accelerated carbonation technology in the treatment of cement-based materials and sequestration of CO2. J. Hazardous Materials 112(3), 193-205.

Fu,Y.,Cai, L. Wu,Y., 2011. Freeze–thaw cycle test and damage mechanics models of alkali-activated slag concrete. Constr. Build. Mater.25 (7), 3144-3148.

Garcia-Lodeiro, I., Carcelen-Taboada, V., Fernández-Jiménez, A., Palomo, A., 2016. Manufacture of hybrid cements with fly ash and bottom ash from a municipal solid waste incinerator, Constr. Build. Mater. 105, 218–226A.

Garg, N., White, C.E., 2017. Mechanism of zinc oxide retardation in alkali-activated materials: an in situ X-ray pair distribution function investigation, J. Mat. Chem. A. Vol. 5 11794–11804.

Gartner, E., Hirao, H., 2015. A review of alternative approaches to the reduction of CO_2 emissions associated with the manufacture of the binder phase in concrete, Cem. Concr. Res. Vol. 78 ,126–142.

Gluth, G.J.G., Lehmann, C., Rübner, K., Kühne, H., 2013. Geopolymerization of a silica residue from waste treatment of chlorosilane production, Mater. Struct. Vol. 46,1291–1298.

Gong, C., Yang, N., 2000. Effect of phosphate on the hydration of alkali-activated red mud–slag cementitious material, Cem. Concr. Res. Vol. 30,1013–1016.

Habert, G.,d'Espinose,J. B. de L., Roussel,N., 2011. An environmental evaluation of geopolymer based concrete production: reviewing current research trends. J. Clean. Prod.19 (11), 1229-1238.

Hadi, M. N. S., Al-Azzawi M., Yu, T., 2018. Effects of fly ash characteristics and alkaline activator components on compressive strength of fly ash-based geopolymer mortar. Constr. Build. Mater. 175, 41-45.

Hajimohammadi, A., Provis, J.L., van Deventer, J.S.J., 2008. One-part geopolymer mixes from geothermal silica and sodium aluminate, Ind. Eng. Chem. Res. Vol. 47,9396–9405.

Hajimohammadi, A., Provis, J.L., van Deventer, J.S.J., 2010. Effect of alumina release rate on the mechanism of geopolymer gel formation, Chem. Mater. Vol. 22 ,5199–5208.

Hajimohammadi, **A., Provis, J.L., van Deventer, J.S.J., 2011.** Time-resolved and spatiallyresolved infrared spectroscopic observation of seeded nucleation controlling geopolymer gel formation, J. Colloid Interface Sci. Vol. 357, 384–392.

Hajimohammadi, A., van Deventer J.S.J., 2017. Characterisation of one-part geopolymer binders made from fly ash, Waste Biom. Valor. 8, 225–233.

Hajimohammadi, A., van Deventer, J.S.J., 2016. Solid reactant-based geopolymers from rice hull ash and sodium aluminate, Waste Biomass Valorization.

Haque, M. A., Bhowmik, S.,Jahin, M. F., 2018. Assessment of curing temperatures to early predict the 28-day mechanical properties for recycle aggregate mixed concrete production. J. Clean. Prod. 174, 1444-1463.

Hardjito, D., Wallah, S.E., Sumajouw, D.M.J., Rangan, B.V., 2004. On the development of fly ash-based geopolymer concrete, ACI Mater. J. Vol. 101 ,467–472.

Hardjito, D., Wallah, S.E., Sumajouw, D.M.J., Rangan, B.V., 2005. Fly ash-based geopolymer concrete, Aust. J. Struct. Eng. Vol. 6,77–86.

Hwang, C.-L., Vo, D.-H.,Tran, V.-A.,Yehualaw, M. D., 2018. Effect of high MgO content on the performance of alkali-activated fine slag under water and air curing conditions. Constr. Build. Mater, 186, 503-513.

Jamieson, E., Kealley, C.S., Van Riessen, A., Hart, R.D., 2016. Optimising ambient setting Bayer derived fly ash geopolymers, Mater. Vol. 9.

Jayaranjan, M.L.D., van Hullebusch, E.D. and Annachhatre, A.P., 2014. Reuse options for coal fired power plant bottom ash and fly ash. Reviews in Environmental Science and Bio/Technology. 13(4) pp. 467-486.

Kalina, L., Bílek, V., Novotnỳ, R., Monček ová, M., Másilko, J., Koplík, J., 2016. Effect of Na3PO4 on the hydration process of alkali-activated blast furnace slag, Mater. Vol. 9.

Ke, X., Bernal, S.A., Ye, N., Provis, J.L., Yang, J., 2015. One-part geopolymers based on thermally treated red Mud/NaOH blends, J. Am. Ceram. Soc. Vol. 98, 5–11.

Khan, M.I., Siddique, R., 2011. Utilization of silica fume in concrete: review of durability properties, Resour. Conserv. Recycl. Vol. 57,30–35.

Kim, M.S., Jun, Y., Lee, C., Oh, J.E., 2013. Use of CaO as an activator for producing a pricecompetitive non-cement structural binder using ground granulated blast furnace slag, Cem. Concr. Res. Vol. 54,208–214.

Koloušek, D., Brus, J., Urbanova, M., Andertova, J., Hulinsky, V., Vorel, J., 2007. Preparation, structure and hydrothermal stability of alternative (sodium silicate free) geopolymers, J. Mater. Sci. Vol. 42,9267–9275.

Komnitsas, K. and Zaharaki, D., 2007. Geopolymerisation: A review and prospects for the minerals industry. Minerals Engineering, 20, 1261-1277.

Kong, D.L.Y., Sanjayan, J.G., 2010. Effect of elevated temperatures on geopolymer paste, mortar and concrete, Cem. Concr. Res. Vol. 40,334–339.

Kovtun, M., Kearsley, E.P., Shekhovtsova, J., 2015. Dry powder alkali-activated slag cements, Adv. Cem. Res. 27, 447–456.

Kuenzel, C., Li, L., Vandeperre, L., Boccaccini, A.R. and Cheeseman, C.R., 2014. Influence of sand of the mechanical properties of metakaolin geopolymers. Construction and Building Materials. 66 pp. 442-446.

Kusbiantoro, A., Ibrahim, M.S., Muthusamy, K., Alias, A., 2013. Development of sucrose and citric acid as the natural based admixture for fly ash based geopolymer, proc, Environ. Sci. Vol. 17, 596–602.

Li, C., Sun, H., Li, L., 2010. A review: The comparison between alkali-activated slag (Si Ca) and metakaolin (Si Al) cements, Cem. Concr. Res. Vol. 40,1341–1349.

Li, X., Wang, Z., Jiao, Z., 2013. Influence of curing on the strength development of calcium-containing geopolymer mortar, Mater. Vol. 6 ,5069–5076.

Liska, M., Al-Tabbaa, A., 2009. Ultra-green construction: reactive magnesia masonry products. Proceedings of the ICE-Waste and Resource Management 162, 185–196.

Luukkonen, T., Abdollahnejad, Z., Yliniemi, J., Kinnunen, P., Illikainen, M., 2018. Comparison of alkali and silica sources in one-part alkali-activated blast furnace slag mortar. J. Clean. Prod. 187, 171-179.

Ma, C., Long, G., Shi, Y., Xie, Y., 2018. Preparation of cleaner one-part geopolymer by investigating different types of commercial sodium metasilicate in China. Journal of Cleaner Production 2018, 636-647

Matalkah, F., Xu, L., Wu, W., Soroushian, P., 2017. Mechanochemical synthesis of one-part alkali aluminosilicate hydraulic cement, Mater. Struct. Vol. 50, 97.

Matalkah, L., Xu, W., Wu, P. Soroushian, 2017. Mechanochemical synthesis of one-part alkali aluminosilicate hydraulic cement, Mater. Struct. 50, 97.

McLellan, B. C., Williams, R. P., Lay, J., van Riessen, A., Corder, G.D., 2011. Costs and carbon emissions for geopolymer pastes in comparison to ordinary Portland cement. J. Clean. Prod., 19, (9–10), 1080-1090.

Memon, F.A., Nuruddin, M.F.L., Demie, S., Shafiq, N., 2012. Effect of superplasticizer and extra water on workability and compressive strength of self-compacting geopolymer concrete, Res. J. Appl. Sci. Eng. Technol. Vol. 4,407–414.

Morrison, J., Jauffret, G., Galvez-Martos, J.L., Glasser, F.P., 2016. Magnesium-based cements for CO2 capture and utilisation. Cement and Concrete Research 85, 183-191.

Mozgawa, W. Deja, J., 2009. Spectroscopic studies of alkaline activated slag geopolymers. Journal of Molecular Structure 924, 434 – 441.

Naghizadeh, A.., Ekolu, S. O., 2017. Pozzolanic materials and waste products for formulation of geopolymer cements in developing countries: a review. Concrete Beton 151, 22-31.

Nematollahi, B., Sanjayan J., 2016. Ambient temperature cured one-part engineered geopolymer composite: a sustainable alternative to engineered cementitious composite, 9th Rilem International Symposium on Fiber Reinforced Concrete.

Nematollahi, B., Sanjayan, J., 2014. Efficacy of available superplasticizers on geopolymers, Res. J. Appl. Sci. Eng. Technol. Vol. 7 ,1278–1282.

Nematollahi, B., Sanjayan, J., Effect of superplasticizers on workability of fly ash based geopolymer, in: R. Hassan, M. Yusof, Z. Ismail, N. Amin, M. Fadzil (Eds.), InCIEC 2013, Springer, Singapore, 2014, pp. 713–719.

Nematollahi, B., Sanjayan, J., Qiu, J., Yang E., 2017. High ductile behavior of a polyethylene fiber-reinforced one-part geopolymer composite: A micromechanicsbased investigation, Arch. Civ. Mech. Eng. Vol.17, 555–563.

Nematollahi, B., Sanjayan, J., Qiu, J., Yang, E., 2017. Micromechanics-based investigation of a sustainable ambient temperature cured one-part strain hardening geopolymer composite, Constr. Build. Mater. Vol. 131, 552–563.

Nematollahi, B., Sanjayan, J., Shaikh, F.U.A., 2014. Comparative deflection hardening behavior of short fiber reinforced geopolymer composites, Constr. Build. Mater.Vol.70, 54–64.

Nematollahi, B., Sanjayan, J., Shaikh, F.U.A., 2015. Synthesis of heat and ambient cured one-part geopolymer mixes with different grades of sodium silicate, Ceram. Int. 41, 5696–5704.

Němeček, J., Šmilauer, V., Kopecký, L., 2011. Nanoindentation characteristics of alkali-activated aluminosilicate materials. Cem. Concr. Compos.33(2), 163-170.

Nie, Q., Hu, W., Ai, T., Huang, B., Shu, X., He, Q., 2016. Strength properties of geopolymers derived from original and desulfurized red mud cured at ambient temperature, Constr. Build. Mater. Vol. 125,905–911.

Novais, R.M., Buruberri, L.H., Ascensao, G., Seabra, M.P., Labrincha, J.A., 2016. Porous biomass fly ash-based geopolymers with tailored thermal conductivity. Journal of Cleaner Production. 119 99-107.

North, M.R. and Swaddle, T.W. (2000). Kinetics of Silicate Exchange in Alkaline Aluminosilicate Solutions, Inorg. Chem., 39, 2661–2665.

Nyale, S. M., Babajide, O. O., Birch, G. D., Böke, N., Petrik, L. F., 2013. Synthesis and characterization of coal fly ash-based foamed geopolymer. Procedia Environmental Sciences 18, 722–730.

Obonyo, E., Kamseu, E., Melo, U.C., Leonelli, C., 2011. Advancing the use of secondary inputs in geopolymer binders for sustainable cementitious composites: a review, Sustain. Vol. 3,410–423.

Palacios, M., Banfill, P.F.G., Puertas, F., 2008. Rheology and setting of alkali-activated slag pastes and mortars: effect if organic admixture, ACI Mater.J. Vol. 105,140–148.

Palacios, M., Houst, Y.F., Bowen, P., Puertas, F., 2009. Adsorption of superplasticizer admixtures on alkali-activated slag pastes, Cem. Concr. Res. Vol. 39,670–677.

Palacios, M., Puertas, F., 2005. Effect of superplasticizer and shrinkage-reducing admixtures on alkali-activated slag pastes and mortars, Cem. Concr. Res. Vol. 35,1358–1367.

Pambudi, N.A., Itoi, R., Yamashiro, R., Syah Alam, B.Y.C.S.S., Tusara, L., Jalilinasrabady, S., Khasani, J., 2015. The behavior of silica in geothermal brine from Dieng geothermal power plant, Indonesia, Geothermics Vol. 54,109–114.

Paramguru, R.K., Rath, P.C., Misra, V.N., 2005. Trends in red mud utilization - a review, Miner. Process. Extr. Metall. Rev. Vol. 26,1–29.

Peng, M.X., Wang, Z.H., Shen, S.H., Xiao, Q.G., 2015. Synthesis characterization and mechanism sofone-part geopolymeric cement by calcinin glow-quality kaolin with alkali, Mater. Struct. Vol. 48,699–708.

Peys, A., Arnout, L., Blanpain, B., Rahier, H., van Acker, K., Pontikes, Y., 2017. Mix-design Parameters and Real-life Considerations in the Pursuit of Lower Environmental Impact Inorganic Polymers, Waste Biomass Valoris. 1–11.

Peys, A., Rahier, H., Pontikes, Y., 2016. Potassium-rich biomass ashes as activators in metakaolin-based inorganic polymers, Appl. Clay Sci. Vol. 119,401–409.

Provis, J.L., 2017. Alkali-activated materials, Cem. Concr. Res. https:// doi.org/10.1016/j.cemconres.2017.02.009.

Provis, J.L., Introduction and scope, in: Provis, Van Deventer, J.L., J.S.J. 2014. (Eds.), Alkali Activated Materials, State-of-the-Art Report, RILEM TC 224-AAM, Springer, Dordrecht, pp. 1–9.

Rashad, A. M., Khalil, M. H., 2013. A preliminary study of alkali-activated slag blended with silica fume under the effect of thermal loads and thermal shock cycles. Construction and Building materials 40, 522-532.

Rashad, A.M., Zeedan, S.R., Hassan, A.A., 2016. Influence of the activator concentration of sodium silicate on the thermal properties of alkali-activated slag pastes, Construction and Building Materials, 102, 811-820.

Rattanasak, U., Pankhet, K., Chindaprasirt, P., 2011. Effect of chemical admixtures on properties of high-calcium fly ash geopolymer, Int. J. Miner. Metall. Mater. Vol. 18, 364.

R. A. Aguilar, O. B. Díaz, and J. I. E. García, "Lightweight concretes of activated metakaolin-fly ash binders, with blast furnace slag aggregates," *Construction and Building Materials*, vol. 24, pp. 1166–1175, 2010.

Saravanan, G., Jayaseher, A. and Kandasamy, S., 2013. Fly ash based geopolymer concrete – A state of the art review. Journal of Engineering Science and Technology Review. 6(1) pp. 25-32.

Sarker, P.K., Kelly, S., Yao, Z., 2014. Effect of fire exposure on cracking, spalling and residual strength of fly ash geopolymer concrete, Mater. Des. Vol. 63,584–592.

Saxena, S. K., Kumar, M., Singh, N.B., 2017. Fire Resistant Properties of Alumino Silicate Geopolymer cement Mortars. Materials Today 4(4E), 5605-5612.

Schneider, M., Romer, M., Tschudin, M., Bolio, H., 2011. Sustainable cement production—present and future, Cem. Concr. Res. Vol. 41,642–650.

Shekhovtsova, J., Kearsley, E.P., Kovtun, M., 2014. Effect of activator dosage, water-to-binder-solids ratio, temperature and duration of elevated temperature curing on the compressive strength of alkali-activated fly ash cement pastes. Journal of the South African Institution of Civil Engineering 56 (3), 44–52.

Shi, H., 2017. Characterization and Modification of the Secondary Copper Smelting Slag for Smooth Operation and Slag Valorization (Ph.D. Thesis), KU Leuven,

Sikandar, M.A., Jo, B.W., Baloch, Z. et al., 2019. Properties of Chemically Synthesized Nano-geopolymer Cement based Self-Compacting Geopolymer Concrete (SCGC)Journal of Wuhan University of Technology-Mater. Sci. Ed. 34, 98-106.

Sturm, P., Gluth, G.J.G., Brouwers, H.J.H., Kühne, H., 2016. Synthesizing one-part geopolymers from rice husk ash, Constr. Build. Mater. Vol. 124,961–966.

Sturm, P., Gluth, G.J.G., Simon, S., Brouwers, H.J.H., Kühne, H., 2016a. The effect of heat treatment on the mechanical and structural properties of one-part geopolymerzeolite composites, Thermochim. Acta 635, 41–58.

Sturm, P., Gluth, G.J.G., Simon, S., Brouwers, H.J.H., Kühne, H., 2016. The effect of heat treatment on the mechanical and structural properties of one-part geopolymer zeolite composites, Thermo chim. Acta. Vol. 635,41–58.

Sturm, P., Greiser, S., Gluth, G.J.G., Jäger, C., Brouwers, H.J.H., 2015. Degree of reaction and phase content of silica-based one-part geopolymers investigated using chemical and NMR spectroscopic methods, J. Mater. Sci. Vol. 50,6768–6778.

Suwan, T., Fan, M., 2017. Effect of manufacturing process on the mechanisms and mechanical properties of fly ash-based geopolymer in ambient curing temperature, Mater. Manuf. Process. Vol. 32,461–467.

Suwan, T., Fan, M., 2017. Effect of manufacturing process on the mechanisms and mechanical properties of fly ash-based geopolymer in ambient curing temperature, Mater. Manuf. Process. Vol. 32,461–467.

Temuujin, J., Minjigma, A., Lee, M., Chen-Tan, N. van Riessen, A. 2011. Characterisation of class F fly ash geopolymer pastes immersed in acid and alkaline solutions. Cem. Concr. Compos. 33(10), 1086-1091.

Temuujin, J., Williams, R., Van Riessen, A., 2009. Effect of mechanical activation of fly ash on the properties of geopolymer cured at ambient temperature, J. Mater. Process. Technol. Vol. 209 ,5276–5280.

Thomas, R. J., Gebregziabiher, B. S., Giffin A., Peethamparan S., 2018. Micromechanical properties of alkali-activated slag cement binders. Cem. Concr. Compos. 90, 241-256.

Topçu, I.B., Toprak, M. U., Uygunoğlu, T., 2014. Durability and microstructure characteristics of alkali activated coal bottom ash geopolymer cement. J. Clean. Prod. 81, 211-217.

Torres-Carrasco, M., Puertas, F., 2017. Waste glass as a precursor in alkaline activation: Chemical process and hydration products. Constr. Build. Mater.139, 342-354.

van Deventer, J.S.J., Feng, D., Duxson, P., 2010. Dry mix cement composition, methods and system involving same, US Patent 7,691,198 B2.

van Deventer, J.S.J., Feng, D., Duxson, P., 2010. Dry mix cement composition, methods and system involving same, US Patent 7,691,198 B2.

Venkatanarayanan, H.K., Rangaraju, P.R., 2013. Material characterization studies on low and high-carbon rice husk ash and their performance in port land cement mixtures, Adv. Civ. Eng. Mat. Vol. 2, 266–287.

Wang, K., Du, L., Lv, X., He, Y., Cui, X., 2017. Preparation of drying powder inorganic polymer cement based on alkali-activated slag technology, Powder Technol. 312, 204–209.

Xu, Z., Jiang, Z., Wu, D., Peng, X., Xu, Y., Li, N., Qi, Y., Li, P., 2017. Immobilization of strontium-loaded zeolite A by metakaolin based-geopolymer. Ceramics International 43(5), 4434-4439.

Yang, K.H., Song, J.K., 2009. Workability loss and compressive strength development of cementless mortars activated by combination of sodium silicate and sodium hydroxide, J. Mater. Civ. Eng. Vol. 21, 119–127.

Yang, K.H., Song, J.K., Ashour, A.F., Lee, E.T., 2008. Properties of cementless mortars activated by sodium silicate, Constr. Build. Mater. Vol. 22, 1981–1989.

Yang, K.H., Song, J.K., Lee, J.S., 2010. Properties of alkali-activated mortar and concrete using lightweight aggregates, Mater. Struct. Vol. 43,403–416.

Ye, N., Chen, Y., Yang, J., Liang, S., Hu, Y., Xiao, B., Huang, Q., Shi, Y., Hu, J., Wu, X., 2016. Co-disposal of MSWI fly ash and Bayer red mud using an one-part geopolymeric system, J. Hazard. Mater. Vol. 318,70–78.

Ye, N., Yang, J., Liang, S., Hu, Y., Hu, J., Xiao, B., Huang, Q., 2016. Synthesis and strength optimization of one-part geopolymer based on red mud, Constr. Build. Mater. Vol. 111, 317–325.

Yip, C. K., Provis, J.L., Lukey, G. C., van Deventer, J.S.J., 2008a. Carbonate mineral addition to metakaolin-based geopolymers. Cem. Concr. Compos. 30, 979–85.

Yip, C.K., Lukey, G.C. Provis, J.L. van Deventer, J.S.J. , 2008b. Effect of calcium silicate sources on geopolymerisation. Cem. Concr. Res. 38(4), 554-564.

Zaidi S F A, Ul Haq E and Nu K r 2017. Synthesis & characterization of natural soil based inorganic polymer foam for thermal insulations. Construction and Building Materials 157, 994-1000,

Zhang, M., Zhao, M., Zhang, G., Mann, D., Lumsden, K., Tao, M., 2016. Durability of red mud-fly ash based geopolymer and leaching behavior of heavy metals in sulfuric acid solutions and deionized water, Constr. Build. Mater. Vol. 124 ,373–382.

Zhang, H. Y., Kodur, V., Qi, S.L.,Cao, L., Wu, B., 2014. Development of metakaolin–fly ash based geopolymers for fire resistance applications. Constr. Build. Mater. 55, 38-45.

Z. Zhang, K. Wang, B. Mo, X. Li, and X. Cui, "Preparation and characterization of a reflective and heat insulative coating based on geopolymers," *Energy and Buildings*, vol. 87, pp. 220–225, 2015.

Zuda, L, Pavlik Z, Rovnaniková, P, Bayer, P, Cˇerny, R. 2006. Properties of alkali activated aluminosilicate material after thermal load. Int J Thermophys 27(4), 1250 –1263

Tierra geológica y materiales industriales de desecho en la producción de cemento ecológico Bajo nivel de emisiones de CO2 y bajo calentamiento global

RESUMEN

Desde el comienzo de la creación del hombre en el universo y cuando inició sus actividades, la tierra comenzó a sufrir. Estas actividades crearon ambientes contaminantes debido a la alta emisión de dióxido de carbono y aumentaron el calentamiento global. De las principales actividades responsables de producir grandes cantidades de emisiones de CO2 en la tierra es la fabricación de cemento. Esta única industria representa más del 5% de las emisiones globales de CO2 provocadas por el hombre; la cantidad de CO2 emitida por la fabricación de cemento es de casi 950 kg de CO2 por cada 1000 kg de cemento producido. El equipo de investigación tiene como objetivo eliminar estas emisiones contaminadas y disminuir el calentamiento global mediante el uso de diferentes técnicas novedosas que utilizan tanto la tierra natural (materiales geológicos) como los materiales industriales de desecho. Se ha realizado un nuevo tipo diferente de aglutinante cementoso respetuoso con el medio ambiente (cemento geopolímero) con propiedades sobresalientes en dureza, resistencia al fuego y a la corrosión. Por otro lado, la utilización de materiales industriales de desecho crea entornos verdes limpios.

Palabras clave: Calentamiento global, Cemento geopolímero, Industria del cemento, Emisiones de CO_2, Materiales geológicos.